CAGS3 RESEARCH PROJECT 3

THE POTENTIAL OF CO$_2$ GEOLOGICAL UTILISATION AND STORAGE IN THE JUNGGAR BASIN AND THE OPPORTUNITIES FOR EARLY DEMONSTRATION PROJECTS IN THE EASTERN JUNGGAR REGION

Leading Institute	Center for Hydrogeology and Environmental Geology Survey, China Geological Survey
Project Leader	Yujie Diao and Jun Li
Date	31 January 2018

CONTENTS

INTRODUCTION

The China Australia Geological Storage of CO_2 (CAGS) Project is a collaborative project that aims to accelerate the development and deployment of geological storage of carbon dioxide in China and Australia. It is managed by Geoscience Australia (GA) and the Administrative Center for China's Agenda 21 (ACCA21, under the Ministry of Science and Technology, MOST) jointly, as the flagship project of all the CCS international cooperation research projects managed by MOST.

At the end of 2015, GA and ACCA21 started the third CAGS project, and the Center for Hydrogeology and Environmental Geology Survey, China Geological Survey (CHEGS) and the Institute of Rock and Soil Mechanics, Chinese Academy of Science, IRSM were funded to study the third work package of CAGS3 — "Evaluation of CO_2 Geological Utilisation Storage in the Junggar Basin and the Opportunities for Early Demonstration Projects in the Eastern Junggar Region". In addition, in March 2017, GA and the China Geological Survey (CGS) signed a "Collaborative Research Project Agreement" to support this study.

According to the technical contract, our task consists of the following three main research components:

1) Theoretical evaluation of the potential of CO_2 Geological Utilisation and Storage (CGUS) in the Junggar Basin, including deep saline aquifer CO_2 storage, depleted oil and gas field CO_2 storage, Carbon Dioxide Enhanced Oil Recovery (CO_2-EOR), Carbon Dioxide Enhanced Coal Bed Methane (CO_2-ECBM) and Carbon Dioxide Enhanced Water Recovery (CO_2-EWR).
2) Capacity evaluation and numerical simulation of CO_2-EWR in selected storage sites in the Eastern Junggar Basin, based on the geological data from outcrop investigations, 2D seismic exploration, logging and downhole testing.
3) Formulation of a proposal for early opportunities for CCUS, based on a study of source-sink matching and early demonstration opportunities in the eastern Junggar region, and consideration of geological security and social conditions.

After two years of research, we completed all the components and accomplished a large number of significant achievements. Furthermore, through participation in CCS capacity training and international workshops, the CCUS research capability of our younger team members has improved greatly. Two senior hydrogeologists carried out collaborative research as academic visitors in Australia, and Dr. Liuqi Wang helped us improve our geological modeling ability.

1. CO₂ EMISSION SOURCES IN THE JUNGGAR BASIN

According to the requirements of the United Nations Framework Convention on Climate Change (UNFCCC), all contracting parties should prepare national greenhouse gas (GHG) inventories in line with the IPCC Guidelines for National Greenhouse Gas Inventories. In 2008, China commenced preparation of the 2005 National Greenhouse Gas Inventory. In order to further strengthen the capacity for preparation of provincial GHG inventories, experts from various government departments and research institutes formulated the Guidelines for the Compilation of Provincial-level Greenhouse Gas Inventories. The inventory compilation generally follows the basic method in the IPCC Guidelines, and draws from the experience of preparing the 1994 and 2005 greenhouse gas inventories of China's energy activities. However, due to the large number of parameters required for the calculation of CO₂ emissions in the inventory, it is difficult to conduct a detailed investigation of the emissions-producing enterprises throughout the entire Junggar Basin under this research project. Therefore, the CO₂ emissions are calculated based on the annual output or annual production capacity of enterprises, and uses the integrated emission factors that take into account fuel combustion and process elements. The locations of these CO₂ emission sources are also adjusted according to remote sensing imagery.

$$\left(E_{CO_2}\right)_{ji} = \left(EF_{ji}\right)\left(P_1\right)_{ji} \qquad (1\text{-}1)$$

$$\left(E_{CO_2}\right)_{ji} = \left(EF_{ji}\right)\left(P_2\right)_{ji}\left(A_{ji}\right)\left(T_{ji}\right) \qquad (1\text{-}2)$$

$$\left(E_{CO_2}\right)_t = \sum_j \sum_i \left(E_{CO_2}\right)_{ji} \qquad (1\text{-}3)$$

Where: $(E_{CO_2})_{ji}$ is the annual CO₂ emissions of the ith enterprise in the jth industry, $(EF)_{ji}$ is the CO₂ integrated emission factor of the enterprise, $(P_1)_{ji}$ is the annual output, $(P_2)_{ji}$ is the production capacity of the enterprise, $(A)_{ji}$ is the utilisation rate, $(T)_{ji}$ is the full load hours of the equipment, and $(E_{CO2})_t$ is the total emissions estimated per industry). When calculating the total emissions of the industry based on the actual output, formula (1-1) is adopted. When calculating the total emissions of the industry based on the annual production capacity, formula (1-2) is adopted.

The emission sources in the Junggar Basin are mainly located at the edge of the basin, especially in the southern region. They are largely concentrated in the Urumqi, Shihezi and Kuitun areas. The total annual emissions of 54 emission sources in the Basin have reached 132.22 Mt. Power plants account for over 50% of emissions both in quantity and annual emissions share, with the total annual emissions of as many as 32 plants reaching 67.51 Mt/a. There are 5 cement plants in this region, with emissions of 28.05 Mt/a, and 12 chemical plants (including coal chemical and petrochemical plants), with emissions of approximately 22.13 Mt/a.
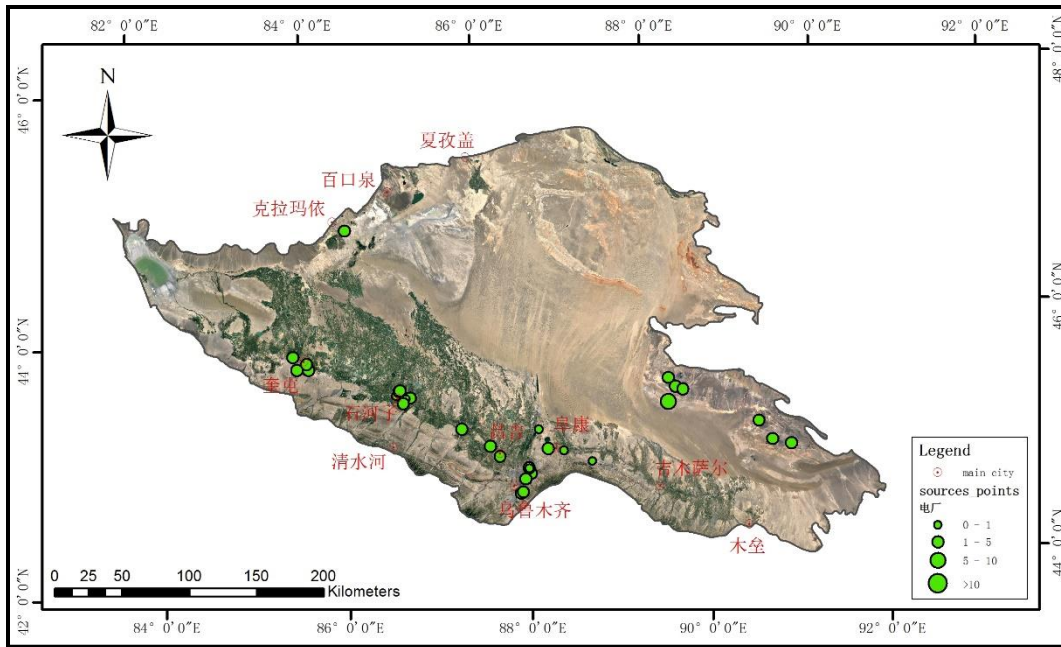
Figure 1.1 Distribution of thermal power plants in the Junggar Basin
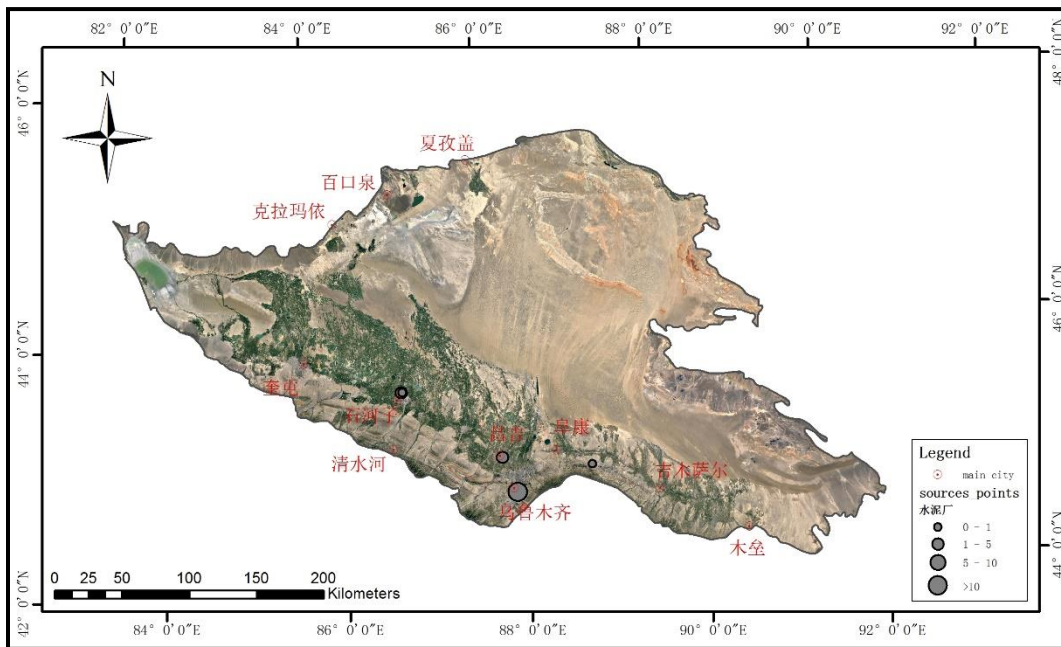

Figure 1.2 Distribution of cement plants in the Junggar Basin
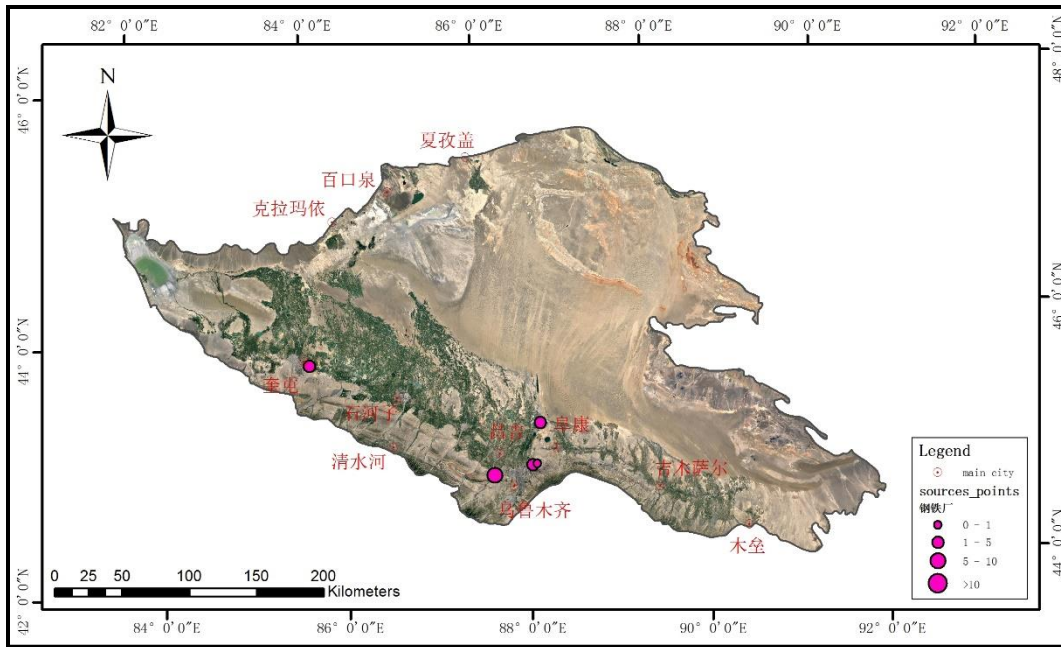
Figure 1.3 Distribution of steel plants in the Junggar Basin
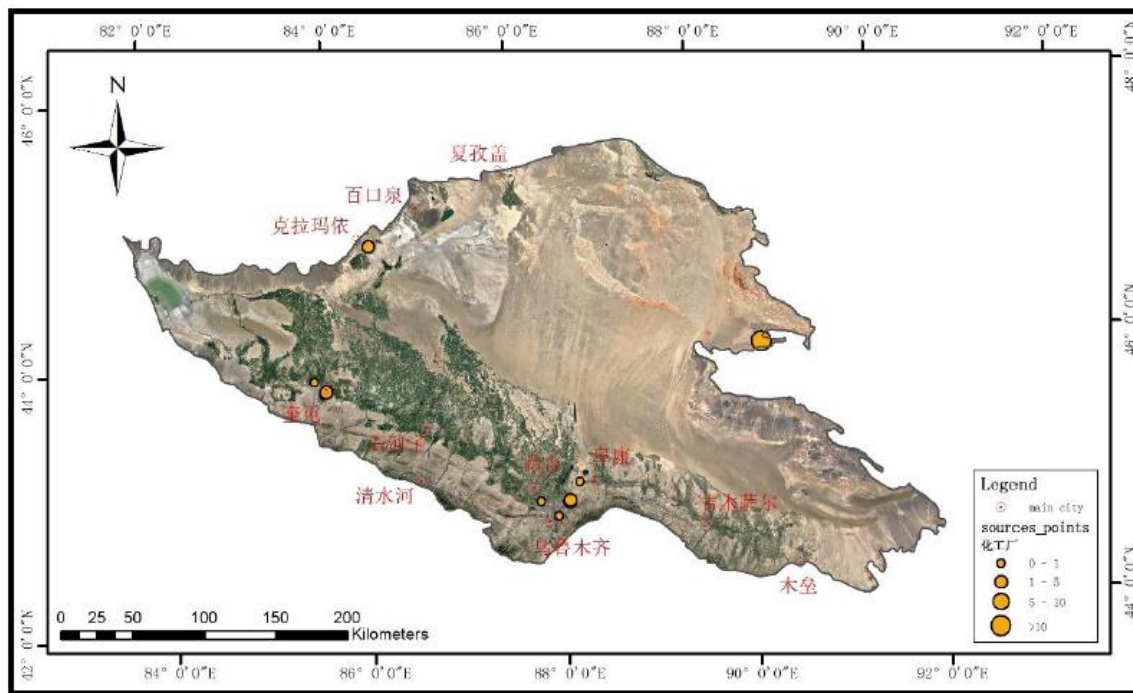
Figure 1.4 Distribution of chemical plants in the Junggar Basin

Table 1.1 Different CO₂ sources in the Junggar Basin

Category	Quantity	Emissions（Mt/a）
Power plant	32	67.51
Steel plant	5	14.53

Cement plant	5	28.05
Chemical plant	12	22.13
Total	54	132.22

Figure 1.5 The proportion of different CO$_2$ emission sources

2. ASSESSMENT OF POTENTIAL AND GEOLOGICAL SUITABILITY FOR TARGET AREA SELECTION

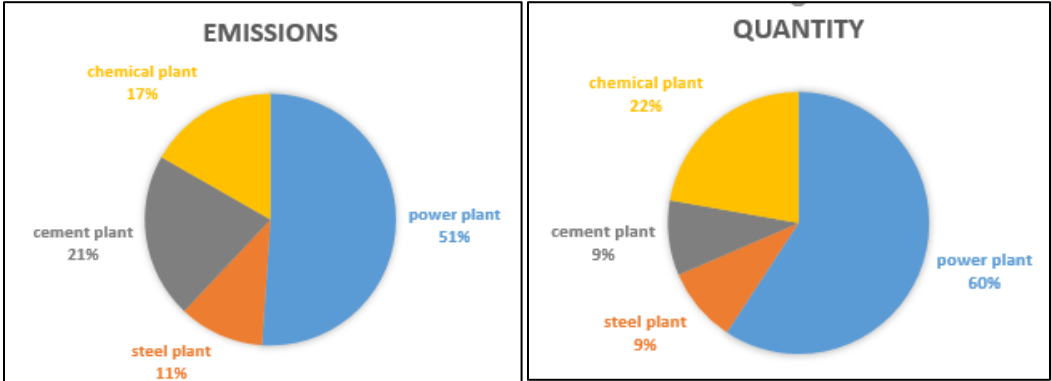Oil and gas fields and coal bed methane (CBM) fields under production could be the target areas on a regional scale for CO_2 geological utilisation or storage. However, for deep saline aquifer CO_2 geological storage or CO_2-EWR, the assessment of potential and geological suitability for target area selection should follow the order of prospective area to target area. This is due to the fast changing lithology and strong heterogeneity in terrestrial sedimentary formations, and also the different distribution of aquifers in lateral and vertical directions. Based on the detailed studies of reservoirs and caprocks in sedimentary basins, and the basic requirements for geological safety, the prospective areas in the Junggar Basin should be selected first, then potential and geological suitability assessment can be carried out for target area selection next.

2.1 METHOD OF ASSESSMENT OF CO_2 GEOLOGICAL UTILISATION AND STORAGE POTENTIAL

2.1.1 DEPLETED OIL FIELD CO_2 GEOLOGICAL STORAGE AND CO_2-EOR
(1) Depleted oil field CO_2 geological storage

The method of assessment of CO_2 geological storage potential of CO_2-EOR is as follows (Goodman, 2011):

$$G_{CO_2} = OOIP/\rho_{oil} \cdot B \cdot \rho_{CO_2} \cdot E_{oil} \qquad (2\text{-}1)$$

Where G_{CO_2} – CO_2 geological storage potential; $OOIP$ – the proven original oil reserves in place, corresponding to the proven oil and gas field geological reserves data of the Ministry of Land and Resources of China (MLR), on a sub-basin scale; ρ_{oil} – oil density at standard atmospheric pressure; B – oil volume factor; ρ_{CO_2} – CO_2 density at reservoir temperature and pressure conditions (according to the Berndt Wischnewski formula); E_{oil} – storage efficiency (or effective coefficient), recommended to be 75% by Li (2009) based on the largest oil production rate of most depleted oil fields in China and the possible amount of CO_2 that could be injected.

(2) CO_2-EOR

The method of assessment of CO_2-EOR storage potential is as follows (Dahowski, 2005):

$$G_{CO_2-EOR} = OOIP/\rho_{oil} \cdot B \cdot E_{oil} \cdot EXTRA \cdot (P_{LCO_2} \cdot R_{LCO_2} + P_{HCO_2} \cdot R_{HCO_2}) \qquad (2\text{-}2)$$

$$API = (141.5/S_g) - 131.5 \qquad (2\text{-}3)$$

Where G_{CO_2-EOR} – CO_2 geological storage potential by using CO_2-EOR technology; $EXTRA$ – enhanced recovery efficiency (see Table 2.1 for values); P_{LCO_2} – the lowest probability of oil recovery (Table 2.2); P_{HCO_2} – the highest probability of oil recovery (Table 2.2); R_{LCO_2} = 2.113 t/m³; R_{HCO_2} = 3.522 t/m³; S_g – specific gravity; other parameters are the same as formula 2-1.

Table 2.1 The value of $EXTRA$ with different API gravity

$EXTRA$ （%）	API
5.3	<31
1.3（API −31）+5.3	31≤ API ≤41
18.3	>41

Table 2.2 Four EOR cases with different depth/pressure and API **gravity**

Depth	API	P_{LCO_2}（%）	P_{HCO_2}（%）
<2000	>35	100	0
	≤35	66	33
>2000	>35	33	66
	≤35	0	100

2.1.2 DEPLETED GAS FIELD CO₂ GEOLOGICAL STORAGE AND CO₂-EGR

(1) Depleted gas field CO₂ geological storage

USDOE (Goodman, 2011) and CSLF (2007) have the same assumptions for assessments of both CO₂-EGR storage potential and CO₂-EOR storage potential. Therefore, the calculation formulas are basically the same:

$$G_{CO_2} = OGIP/\rho_{gasstd} \cdot B \cdot \rho_{CO_2} \cdot E_{gas} \qquad (2\text{-}4)$$

Where $OGIP-$ the proven original natural gas reserves in place, corresponding to the proven oil and gas field geological reserves data of the MLR; ρ_{gasstd} – gas density under standard atmospheric pressure; B – natural gas volume factor; E_{gas} – storage efficiency (effective coefficient), 75% (Li, 2009); other parameters are the same as formula 2-1.

(2) CO₂-EGR

Whether CO₂-EGR technology is feasible or not, we can evaluate the storage potential of CO₂ using the following formula:

$$G_{CO_2-EGR} = OGIP/\rho_{gasstd} \cdot B \cdot \rho_{CO_2} \cdot E_{gas} \cdot C \qquad (2\text{-}5)$$

Where G_{CO_2-EGR} – CO₂ geological storage potential by using CO₂-EGR technology; C – reduction coefficient, compared with depleted gas storage, Li recommends that it be 63% (Li, 2009); other parameters are the same as formula 2-4.

2.1.3 Unmineable coal seam CO₂ storage and CO₂-ECBM

(1) Unmineable coal seam CO₂ storage

The formula to calculate the storage potential is as follows:

$$G_{CO_2} = G_{CBM} \cdot R_{CO_2/CH_4} \cdot \rho_{CO_2std} \cdot E_{coal} \qquad (2\text{-}6)$$

Where G_{CBM} – coal bed methane reserves (MLR has only published prospective reserves, which are less credible than the oil and gas reserves); R_{CO_2/CH_4} – the absorption capacity ratio of CO₂ and CH₄ in the coal seam; E_{coal} – storage efficiency (effective coefficient); other parameters are the same as formula 2-4.

The values of R_{CO_2/CH_4} and E_{coal} were proposed by USDOE (2003) and Goodman (2011), as shown in Table 2.3 and Table 2.4.

Table 2.3 The values of R_{CO_2/CH_4} **and** C **of different types of coal（USDOE, 2003）**

Types of coal	R_{CO_2/CH_4}	C

Lignite	10	1.00
Non-caking coal	10	0.67
Weakly caking coal	10	1.00
Long flame coal	6	1.00
Gas coal	3	0.61
Fat coal	1	0.55
Coking coal	1	0.50
Lean coal	1	0.50
Meager coal	1	0.50
Anthracite	1	0.50

Table 2.4 Storage efficiency of unmineable coal seams (Goodman, 2011)

P_{10}	P_{50}	P_{90}
21%	37%	48%

(2) CO_2-ECBM

The formula to calculate the geological storage potential of CO_2-ECBM is as follows:

$$G_{CO_2-ECBM} = G_{CBM} \cdot R_{CO_2/CH_4} \cdot \rho_{CO_2 std} \cdot E_{coal} \cdot C \tag{2-7}$$

Where G_{CO_2-ECBM} – CO_2 geological storage potential by using CO_2-ECBM technology; C – recovery coefficient of different types of coal; other parameters are the same as formula 2-6.

2.1.4 Deep saline aquifer CO_2 storage and CO_2-EWR

The formulas to calculate CO_2-EWR and storage-only saline aquifer geological storage potential are the same as follows:

$$G_{CO_2} = A \cdot h \cdot \varphi_e \cdot \rho_{CO_2} \cdot E_{saline} \tag{2-8}$$

Where A – reservoir distribution area; h – reservoir thickness; φ_e – saline aquifer average effective porosity; E_{saline} – storage efficiency (effective coefficient), shown in Table 2.5; other parameters are defined above.

Table 2.5 CO_2 storage efficiency coefficients E_{saline} (Bachu, 2015)

Lithology	P_{10}	P_{50}	P_{90}
Clastics	1.2%	2.4%	4.1%
Dolomite	2.0%	2.7%	3.6%
Limestone	1.3%	2.0%	2.8%

2.2 METHOD OF SUITABILITY ASSESSMENT FOR SALINE AQUIFER STORAGE TARGET SELECTION

2.2.1 MATHEMATICAL MODEL
(1) GIS superimposed multi-source information assessment technology

Superimposed multi-source information assessment technology is an integrated method of processing multi-source geological data. Based on the two-dimensional space determined by geographical coordinates, the unity of the geographical coordinates within the same region but with different information, i.e. the so-called spatial registration, is achieved, which is performed by using geographic information software (ArcGIS or MapGIS).

(2) Mathematical model

The selected prospective areas undergo the GIS spatial analysis into grids of 1500 m × 1500 m. The thematic information map prepared for each factor is screened by key veto factors. In this way, a single factor unfit for CO_2 geological storage is identified, so as to abandon the grids that are unsuitable for deep saline aquifer CO_2 storage.

Then, GIS spatial analysis and evaluation is carried out using formula 2-9.

$$P = \sum_{i=1}^{n} P_i A_i (i = 1,2,3.....n) \qquad (2\text{-}9)$$

Here, P– suitability score of unit for CO_2 geological storage; n– the total number of evaluation factors; P_i – given point of the i th evaluation index; A_i – weight of the i th evaluation index.

Single metric suitability rating: "good" 9 points, "average" 5 points, and "poor" 1 point.

The evaluated suitability rating: "highly suitable" value range $7 \leq P \leq 9$, "suitable" $5 \leq P < 7$, "less suitable" $3 \leq P < 5$, and "unsuitable" $1 \leq P < 3$.

2.2.2 INDEX SYSTEM FOR GEOLOGICAL SUITABILITY ASSESSMENT

As shown in Table 2.6, the index system for geological suitability has three hierarchies. The index weights at all levels are determined using the Analytic Hierarchy Process (AHP) (Saaty, 1980, 1985).

Table 2.6 Index system for geological suitability assessment to select suitable targets for deep saline aquifer CO_2 storage

Level one index	Weight	Level two index	Weight	Level three index	Weight	Good	Normal	Poor	Key veto factor
Reservoir conditions and storage potential	0.50	Characteristics of the best reservoir	0.60	Lithology	0.07	Clastic	Mix of Clastic and Carbonate	Carbonate	
				Single layer thickness h/m	0.11	≥80	$30 \leq h < 80$	$10 \leq h < 30$	< 10
				Sedimentary facies	0.36	River, Delta	Turbidity, Alluvial fan	Beach bar, Reef	
				Average porosity φ/%	0.20	≥15	$10 \leq \varphi < 15$	$5 \leq \varphi < 10$	< 5
				Average permeability k/mD	0.27	≥50	$10 \leq k < 50$	$1 \leq k < 10$	< 1
		Storage potential	0.40	Storage potential per unit area G (10^4 t/km²)	1.00	≥100	$10 \leq G < 100$	< 10	
Geological safety	0.50	Characteristics of the main caprock	0.62	Lithology	0.30	Evaporites	Argillite	Shale and dense limestone	
				Thickness h/m	0.53	≥100	$50 \leq h < 100$	$10 \leq h < 50$	< 10
				Depth D/m	0.11	<1000	$1000 \leq D \leq 2700$	>2700	
				Buffer caprock above main caprock	0.06	Multiple sets	Single set	None	
		Hydrodynamic conditions	0.24	Hydrodynamic conditions	1.00	Groundwater high-containment area	Groundwater containment area	Groundwater semi-containment area	Groundwater open area
		Seismic activity	0.14	Peak ground acceleration	0.50	< 0.05 g	0.05 g, 0.10 g	0.15 g, 0.30 g	≥0.40 g

				Development degree of fractures	0.50	Simple	Moderate	Complex	Within 25 km of active faults

Details of the assessment indexes are described below:

(1) Characteristics of the best reservoir

Depth: Only if the theoretical storage depth is more than 800 metres can CO_2 enter the supercritical state, normally lower than 3,500 metres.

Lithology: According to the engineering experiences of existing commercial-scale CO_2 geological storage projects (e.g., Haddadji, 2006; Wright, 2007; Skalmeraas, 2014), the reservoir characteristics of oil and gas fields in China (Li, 2002) and the engineering verification by the Shenhua CCS demonstration project in the Ordos Basin (Wu, 2013), clastic reservoirs are generally better than carbonate reservoirs.

Single layer thickness: Because of terrestrial sedimentary facies in most formations in onshore basins within China, it is difficult to find large thick aquifers for CO_2 storage similar to those in the Sleipner project in Norway. The minimum single layer thickness of reservoirs recommended in this paper is 10 m.

Sedimentary facies: Most Cenozoic sedimentary basins in China are terrestrial sedimentary formations. The main part of the reservoir is the deltaic sand body, followed by the turbidite sand and alluvial fan glutenite body, and finally the sand beach dams and a small amount of reef.

Porosity and permeability: Low porosity and permeability is a special feature in terrestrial sedimentary oil and gas reservoirs, and saline aquifers in China. Generally, for both the clastic and carbonate rock reservoirs, the porosity should be greater than or equal to 5% and permeability should be greater than or equal to 1 mD (e.g. Bachu, 2003; IPCC, 2005; Oldenburg, 2008; Diao, 2012).

(2) Characteristic of the main caprock

Lithology: The most common caprocks of oil and gas fields in China are argillite (mudstone, shale) and evaporites (gypsum, rock salt), followed by carbonate rocks (marl, argillaceous dolomite, compact limestone, dense dolomite) and frozen genesis caps. Sometimes there are local chert layers, seams, dense volcanic rocks and intrusive rock caps.

Thickness: There are certain relationships between cap thickness and the size and height of the reservoir. With the combination of existing cap thickness grading standards (Diao, 2012) and considerations of the differences between CO_2 and oil and gas, the reference criteria for grading the classification of CO_2 geological storage cap thickness can be specified. The minimum thickness of CO_2 geological storage caprocks recommended in this paper is 10 m.

Burial depth: The cap type is argillaceous rocks. The diagenesis has different effects on the performance of the caprock at different stages (Liu, 2008). When the burial depth of argillaceous rocks is less than 1,000 m, the diagenetic degree is poor and the sealing mainly relies on the capillary pressure. The porosity and permeability are good but with poor plasticity, and sealing ability is generally poor. At the burial depth of 1,000–2,700 m, the diagenesis is enhanced, mineral particles inside the argillaceous rock become more compacted, the porosity and permeability deteriorate, the plasticity increases, the capillary flow capacity declines, sealing ability improves, and there is abnormal sealing pressure. When the burial depth is greater than 2,700 m, it is equivalent to the tightly compacted stage of argillite. As the degree of diagenesis further increases, the plasticity decreases and fragility increases. With the increase in abnormal pressure, microcracks appear on the argillaceous rocks, and capillary sealing ability deteriorates.

The "buffer cap" above the main caprock: When the CO_2 breaks through the main cap, the "buffer cap" above the main cap has to provide a certain sealing capability to reduce or prevent the escape of CO_2.

(3) Geological safety

Hydrodynamic conditions: Ye (2001) divided the effect of hydrogeological conditions that control coal bed methane into three categories: hydraulic transport dissipation effect, hydraulic seal effect and hydraulic block effect. The more closed the hydrogeological conditions, the more favorable they are for CO_2 geological storage. Basin sections with complex geological structure and powerful water alternation are not suitable CO_2 geological storage prospective areas due to the high degree of hydrogeology and strong groundwater activities.

Peak ground acceleration: The " Seismic Ground Motion Parameter Zonation Map of China" (GB 18306-2001), which shows the Chinese seismic zonation map, its technical elements and user provisions, is also applicable to CO_2 geological storage construction projects. The greater the peak ground acceleration, the more unfavorable it is for CO_2 geological storage. Generally, the peak ground acceleration should be less than 0.40 g. In addition, active faults are not only CO_2 leakage pathways but also cause damage to the strata continuity, resulting in CO_2 leakage through the caprock. According to the "Evaluation of Seismic Safety for Engineering Sites" (GB 17741-2005), the identification of active faults has to be made within a 5 km range of Grade I sites and their extensions, and the seismic safety evaluation should extend to a 25 km radius. Therefore, it is inappropriate for areas within 25 km of an active fault to be a prospective area.

Development degree of fractures: CO_2 could leak by tectonic pathways including faults, fractures and ground fissures (e.g., IPCC, 2005; Pruess, 2008; Lemieux, 2011; Diao, 2015). The more complex the fault system, the more unfavorable it is for CO_2 geological storage. In addition, there has been more frequent seismic activity in the Sichuan Basin in recent years.

(4) Storage potential per unit area

Guo (2014) evaluated the national scale potential of CO_2 geological storage in deep saline aquifers of 390 onshore basins in China, supported by the China Geological Survey. As shown in Figure 2.1, the potential of CO_2 geological storage in deep saline aquifers in most of the sedimentary basins is generally 50×10^4 - 100×10^4 t. A small number of basins have a storage potential of less than 10×10^4 t or more than 100×10^4 t.
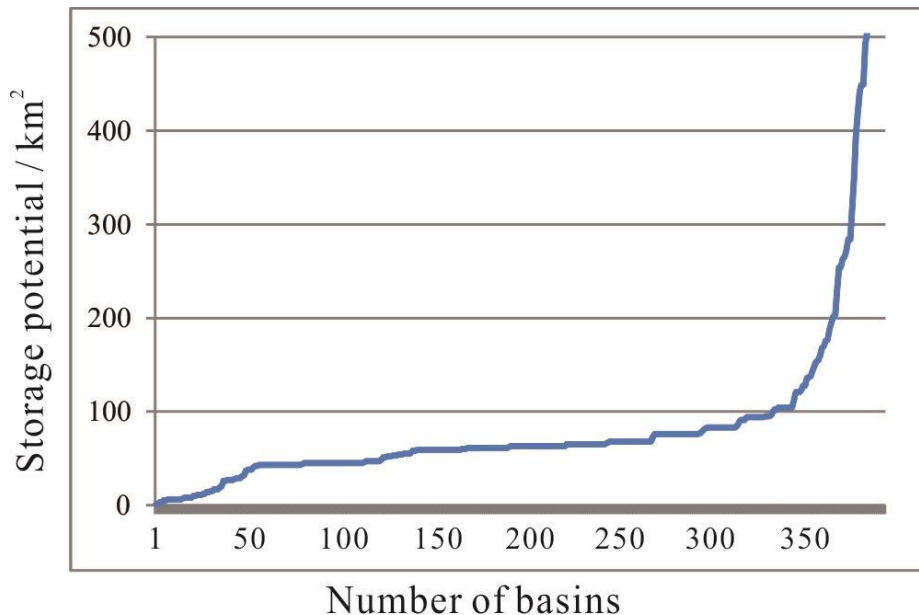

Figure 2.1 The statistical profile of CO_2 geological storage potential per square kilometre of 390 onshore basins in China

2.3 RESULTS

13

2.3.1 POTENTIAL

The results of CO₂ geological utilisation and storage potential are shown in the Table 2.7.

Table 2.7 Summary of CO₂ geological utilisation and storage potential in the Junggar Basin

CGUS Technology	Potential (10^8t)	Credibility
Enhanced oil recovery, CO₂-EOR	1.48	Effective, Credible
Depleted oil field CO₂ storage	13.45	Effective, Credible
Enhanced gas recovery, CO₂-EGR	0.09	Effective, Credible
Depleted gas field CO₂ storage	0.16	Effective, Credible
Enhanced coal bed methane, CO₂-ECBM	22.81-52.15 40.2 expected	Theoretical, Less Credible
Unmineable coal seam CO₂ storage	34.05-77.83 60 expected	Theoretical, Less Credible
CO₂-EWR/deep saline aquifer	480.27-1640.93 960.55 expected	Theoretical, Less Credible

Storage potential per unit area for each prospective area is shown in Figure 2.3.

Figure 2.2 Reservoirs and caprocks for deep saline aquifer CO₂ geological storage
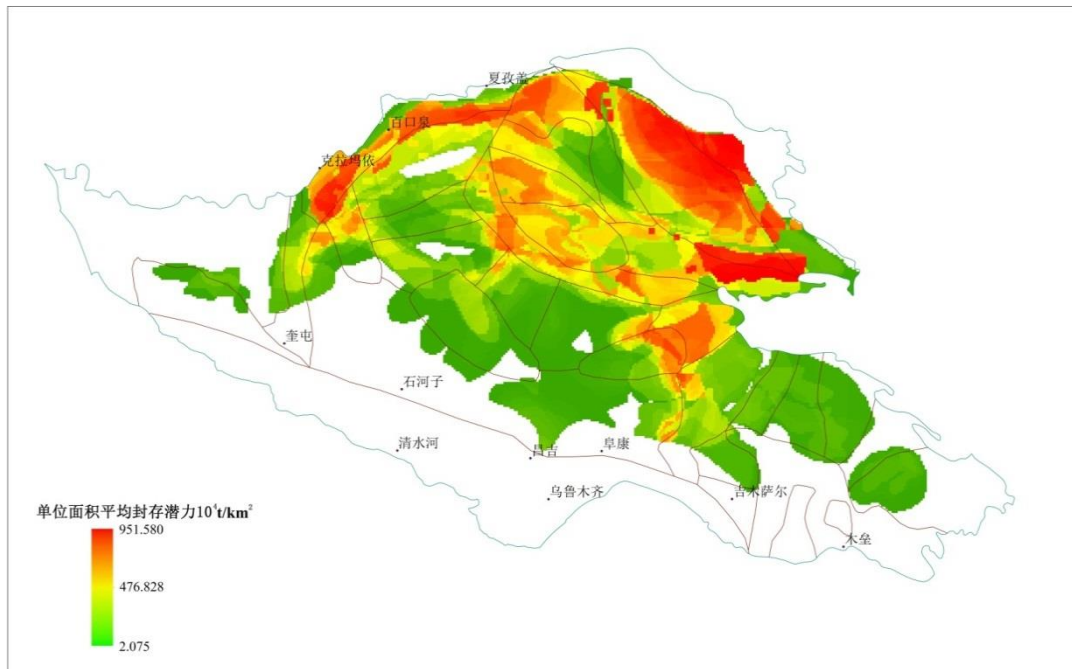

Figure 2.3 Storage potential per unit area of prospective areas in the Junggar Basin
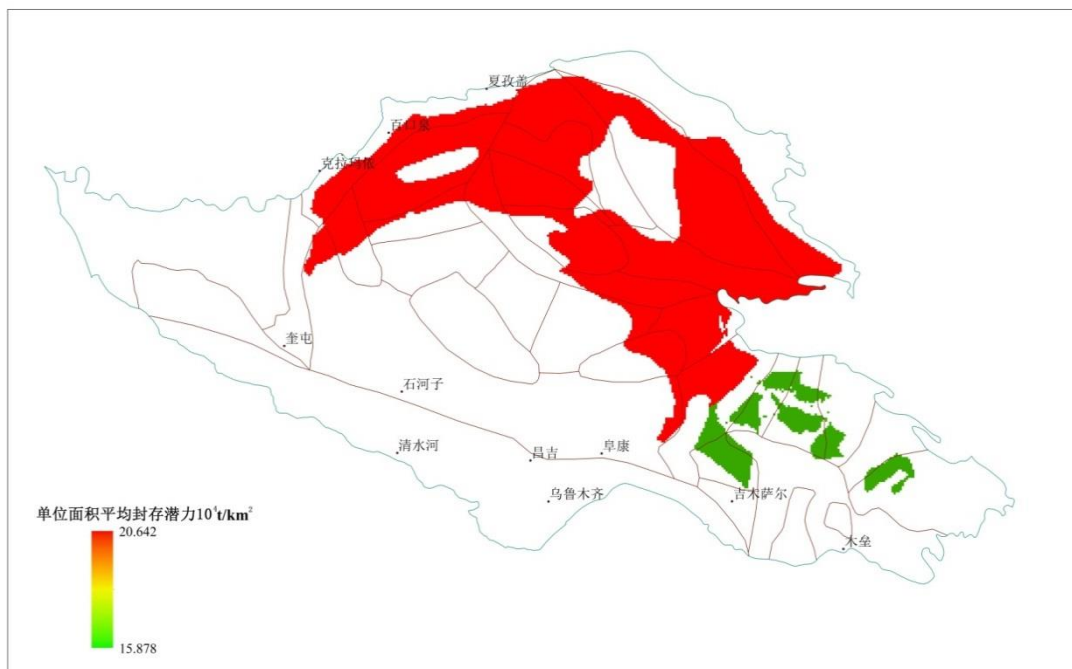

Figure 2.4 Storage potential per unit area of Second Sandstone Formation in Second Member of Sangonghe Formation
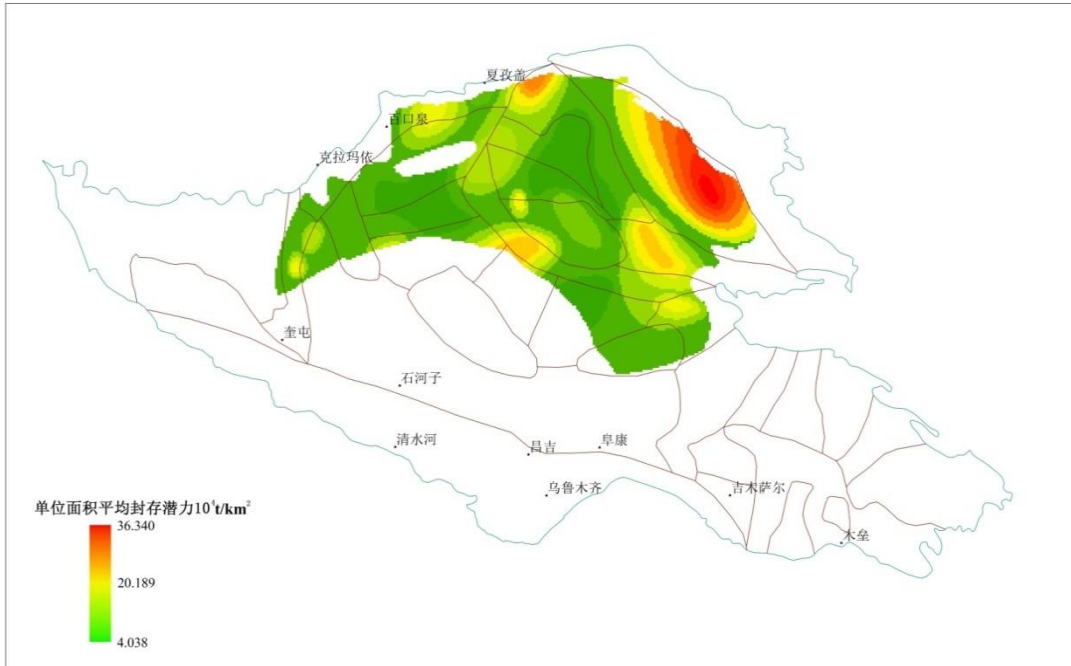
Figure 2.5 Storage potential per unit area of glutenite at the bottom of Qingshuihe Formation

2.3.2 TARGETS

For CO₂ enhanced oil and gas recovery (CO₂-EOR, EGR), coal bed methane recovery (CO₂-ECBM), or storage in depleted oil, gas and unmineable coal seams, existing oil fields, gas fields or coal seams could be the target areas on a regional scale. However, for CO₂ enhanced water recovery (CO₂-EWR) or storage-only deep saline aquifer storage, the assessment of potential and geological suitability for target area selection should follow the order of prospective area to target area.
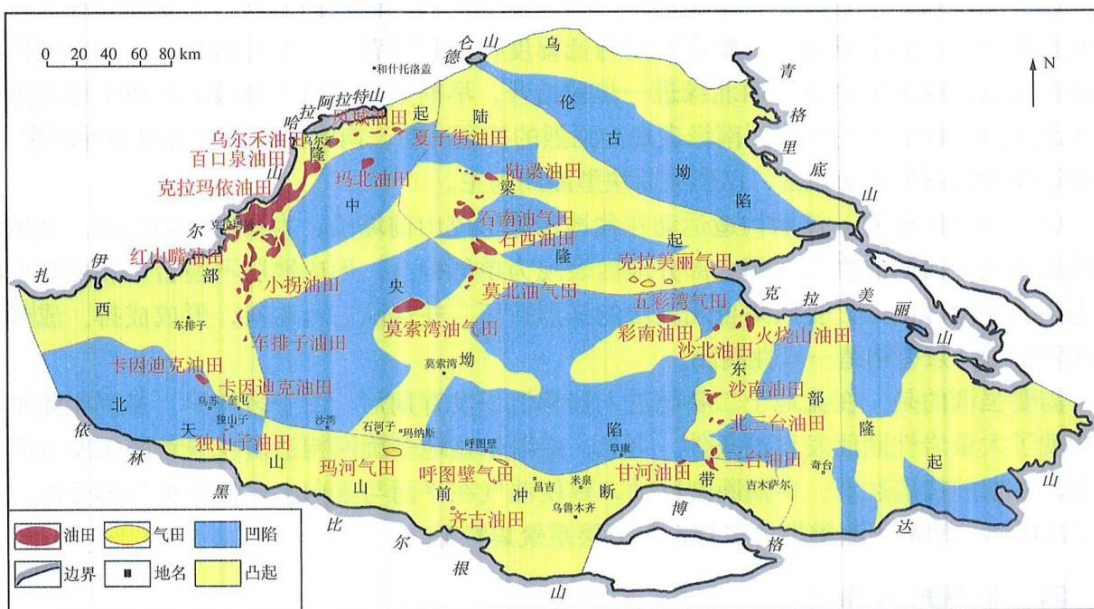

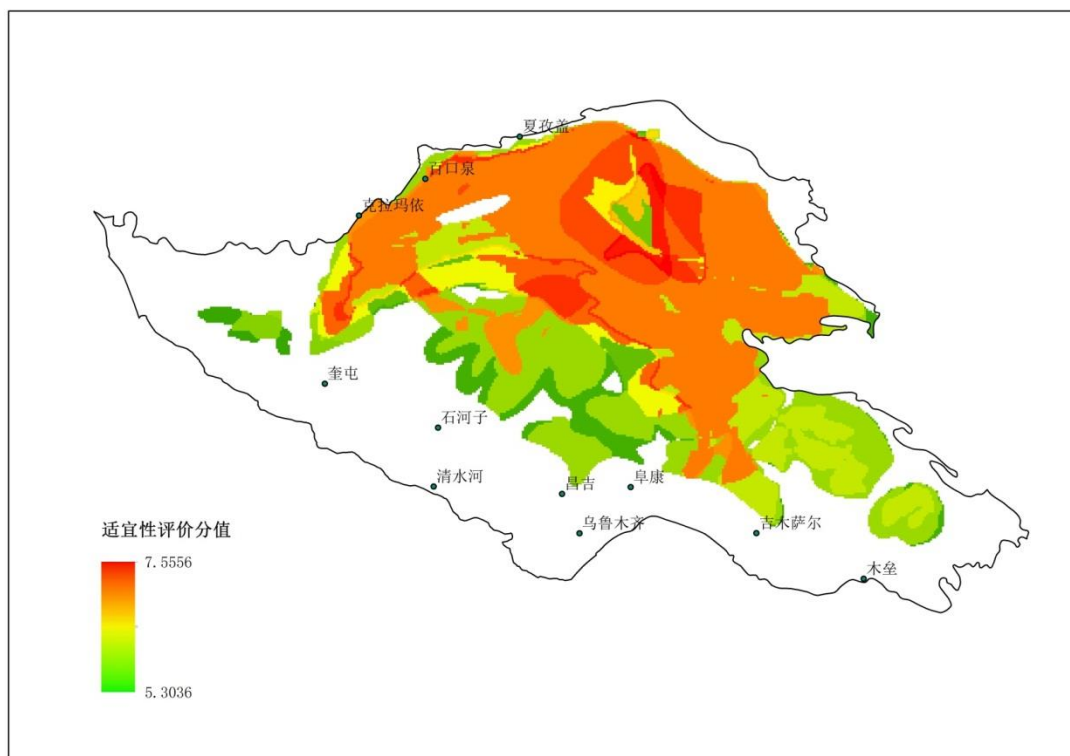**Figure 2.6 Oil and gas fields in the Junggar Basin**

Figure 2.7 Targets for deep saline aquifer CO$_2$ geological storage or CO$_2$-EWR

3. CO₂ SOURCE-SINK MATCHING AND EARLY OPPORTUNITIES IN THE JUNGGAR BASIN

3.1 SITE GEOGRAPHIC INFORMATION DATABASE

In order to carry out source-sink matching analysis and CO_2-EWR technical and economic analysis, a geographic information database of the Junggar Basin was established, which included land cover, digital elevation models (DEM), surface gradient, population density and remote sensing imaging, etc.
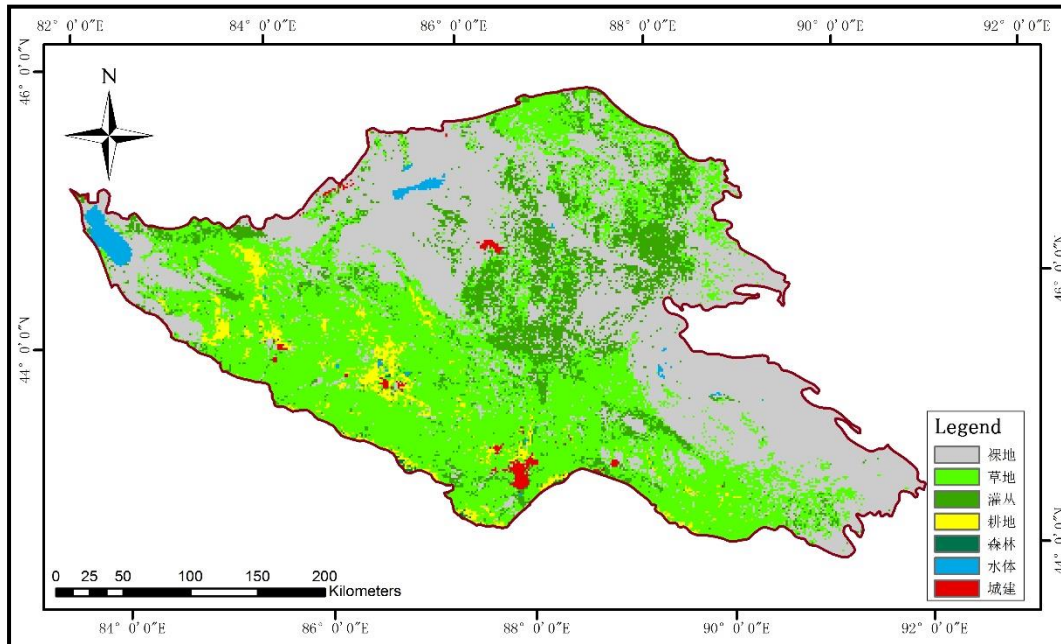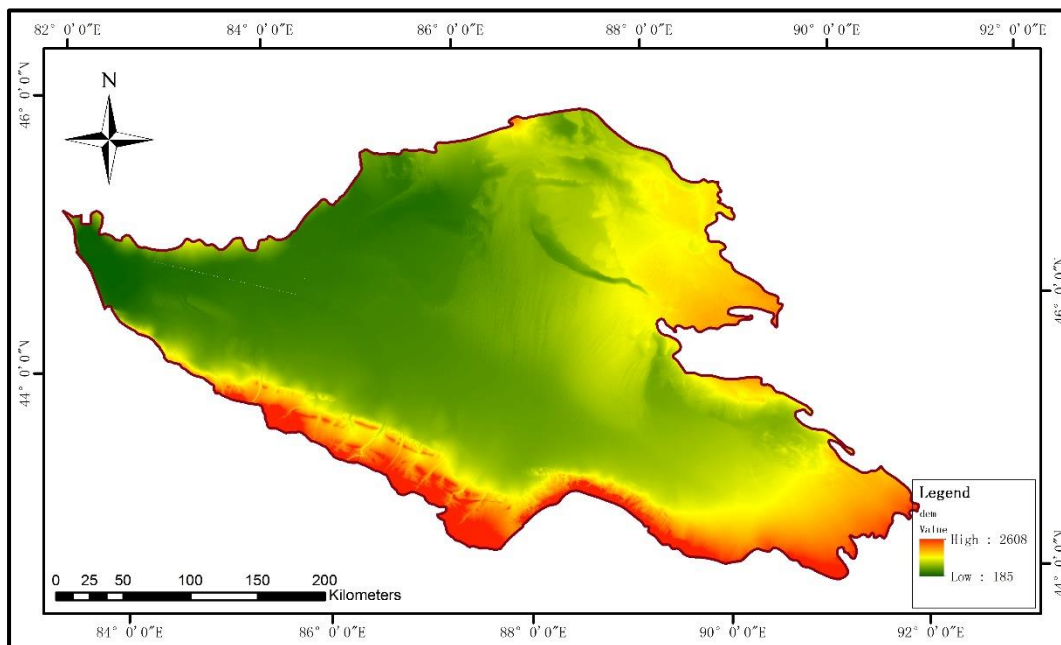

Figure 3.1 Land cover of the Junggar Basin

Figure 3.2 DEM of the Junggar Basin
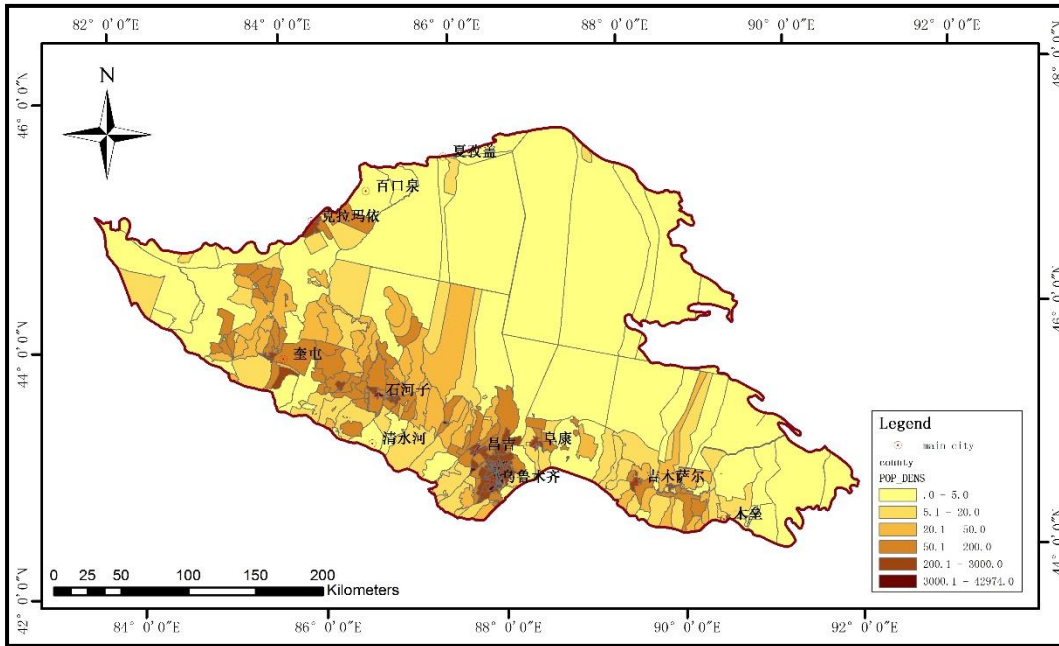
Figure 3.3 Population density of the Junggar Basin（unit：people/km²）
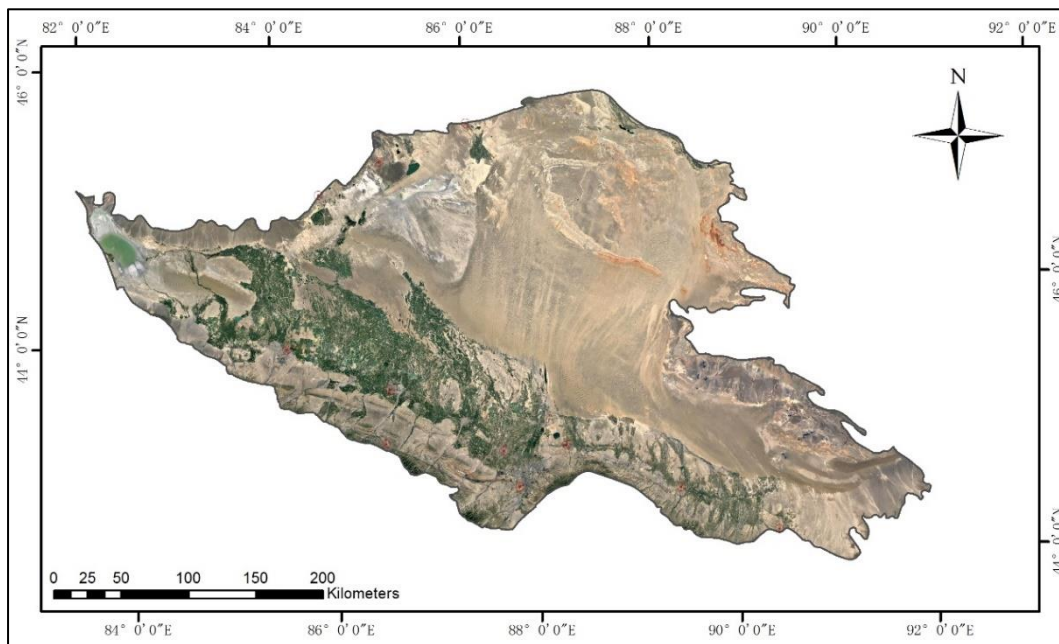
Figure 3.4 Remote sensing image of the Junggar Basin

3.2 METHOD OF SOURCE-SINK MATCHING

Carbon dioxide geological utilisation and storage (CGUS) technology is a complex system. The essence of CGUS source-sink matching is a mixed integer programming problem, which involves considering all of the influencing factors systematically and then optimising the selection of CO_2 emission sources, storage sites, as well as their transportation paths.

19

The "cost surface" is analysed by ArcGIS 10.3 software, considering the impacts of all relevant factors. Different layers in the GIS database are assigned suitable values, as shown in Table 3.1. Subsequently, these layers are calculated based on formula (3-1), then rasterized to obtain the cost surface.

$$P = \sum_{i=1}^{n} P_i A_i (i = 1,2,3.....n)$$

(3-1)

Where P is the total value; n is the number of layers; P_i is the given value of the ith layer; A_i is the ith layer.

Table 3.1 Values of different layers

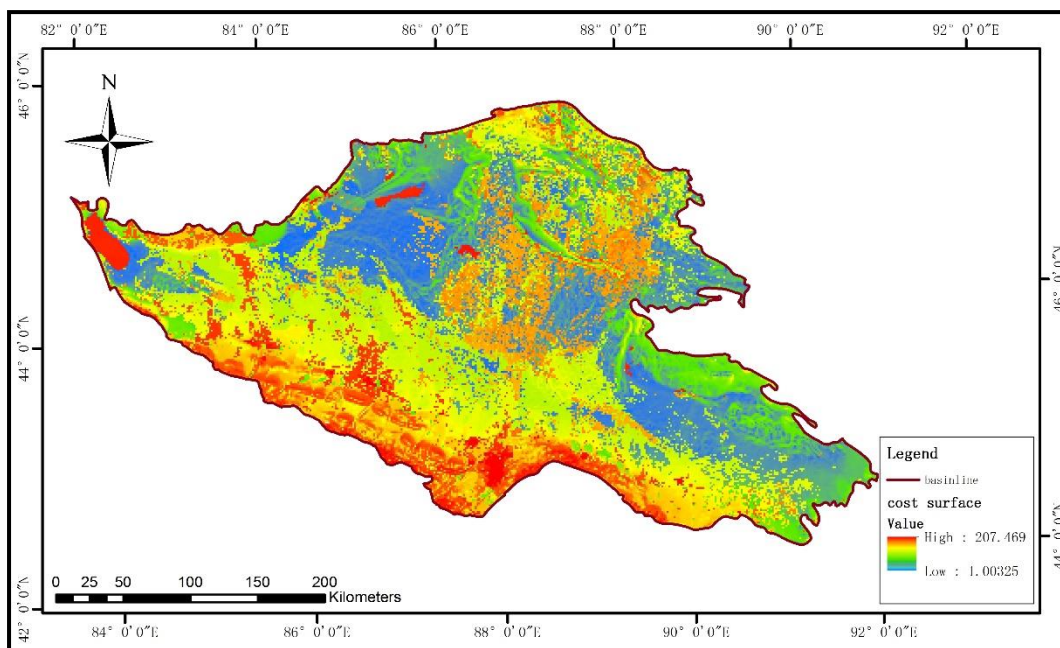| Layer	Value
Water	11
Forest	10
Bush	5
Grass	3
Cultivated land	8
Barren land	1
Urban construction area	14
Population density	$(0 \sim 156)$
Surface gradient	$(0 \sim 13)$

Figure 3.5 Cost surface of the Junggar Basin

Using the "cost surface" as the base map, we can use the Cost-Weighted Distance Analysis Tool and Cost Paths in the ArcGIS Spatial Analysis Tool to analyse the relative cost of "transportation routes" in the Basin.
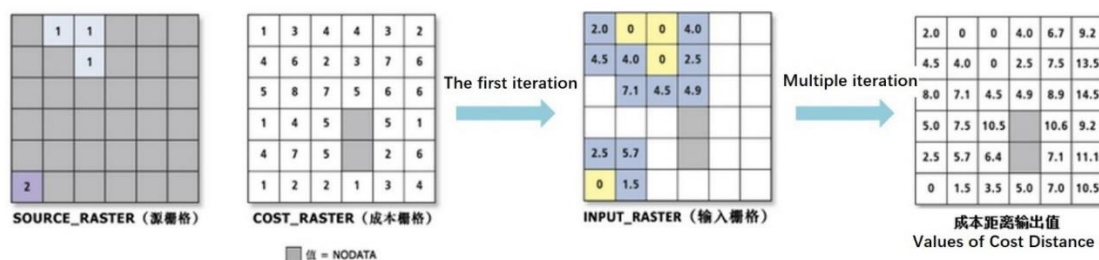

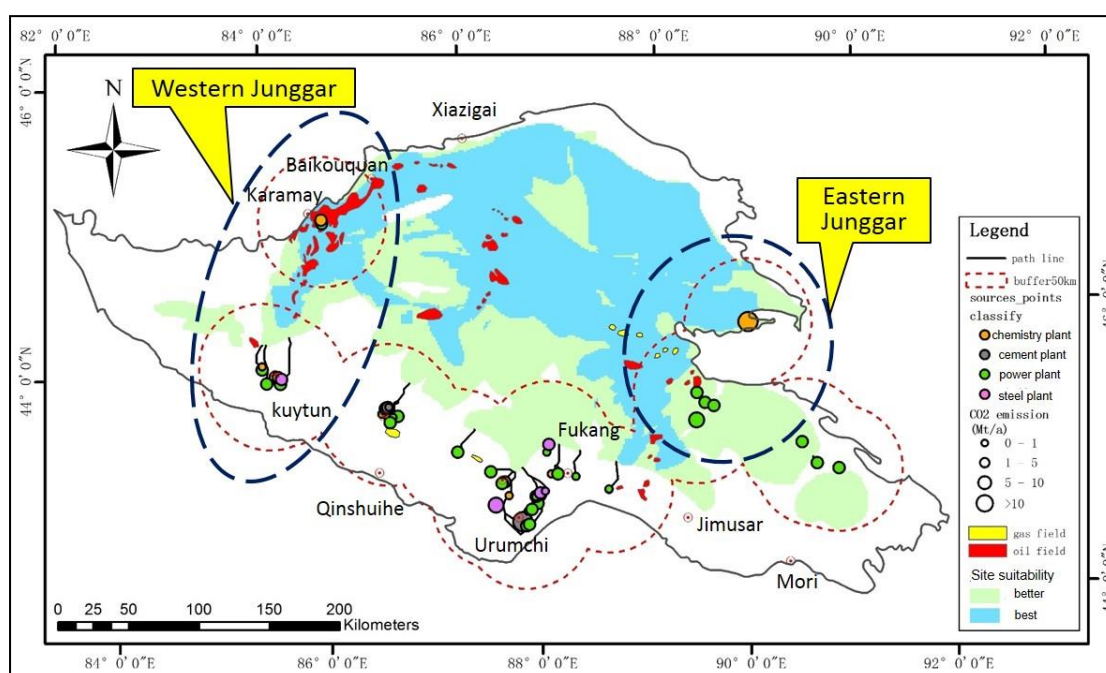**Figure 3.6 Schematic diagram of cost distance tool**

Figure 3.7 Junggar Basin source-sink matching results

As shown in Figure 3.7, the Junggar Basin has good source-sink matching results. All CO_2 emission points could be matched to suitable storage sites within a range of no more than 50 kilometers. In fact, the longest route is about 32.5km. In many areas, CO_2 can be captured and stored in the surrounding areas, such as in Karamay, Fuyun and Wucaiwan Industrial Park in the Eastern Junggar Basin. The early demonstration opportunity analysis of the Junggar Basin should also consider the current local industry deployment and the willingness of enterprises to participate, together with the capture cost (which accounts for most of the cost in the overall CCUS process).

3.2.1 THE EARLY DEMONSTRATION OPPORTUNITIES IN WESTERN JUNGGAR BASIN

Western Junggar Basin is suitable for CO_2-EOR demonstration projects. There are several oilfields with large reserves, especially Karamay oilfield, Baikouquan oilfield and Hongshanzui oilfield. Among these, Karamay oilfield is the largest both in terms of area and reserves. Around these oilfields, there are 12 CO_2 emission points located in Karamay and Kuitun, including chemical plants, power plants and steel plants, with emissions of 12.01 Mt/a. In addition, Xinjiang Dunhua Petroleum Technology Co., Ltd., located in Karamay, has built a

CO_2 capture device (0.1 Mt/a capture capacity). In addition, there are another two projects under construction, a CO_2 capture device at the Tahe Refinery (0.1 Mt/a) and a CO_2 low-temperature distillation capture device for Changqing Oilfield (0.1 Mt/a). Considering the capture cost, chemical plants are preferred as CO_2 emission sources, so Karamay Petrochemical Co. can be the CO_2 emission source.

Table 3.2 The main CO_2 emission points in Western Junggar Basin

Class	Number	Emissions（Mt/a）
Chemical plant	6	3.25
Power plant	5	7.08
Steel plant	1	1.68
Total	12	12.01

Table 3.3 Inventory of main CO_2 emission points in Western Junggar Basin

| Name	Location	Class	Emissions （Mt/a）
Kuishan Baota Power Station	Kuitun	Power plant	1.48
Duzishan Petrochemical Power Station	Duzishan	Power plant	1.21
Kuitun Thermal Power Plant	Kuitun	Power plant	1.48
SPI Wusu Thermal Power Plant	Wusu County	Power plant	1.34
Guodian Karamay Power Generation Co., Ltd.	Karamay	Power plant	1.57
Xinjiang Kunyu Steel Co., Ltd.	Kuitun	Steel plant	1.68
CNPC Dushanzi Petrochemical Branch	Karamay	Chemical plant	0.81
Xinjiang Dushanzi Tianli High & Newtech Co., Ltd.	Karamay	Chemical plant	0.04
Xinjiang Kuitun Jinjiang Chemical Co., Ltd.	Kuitun	Chemical plant	1.05
Wusu Xinhai Chemical Co., Ltd. Ltd.	Wusu City	Chemical plant	0.02
Huatai Petrochemical Co., Ltd.	Wusu City	Chemical plant	0.12
Karamay Petrochemical Co., Ltd.	Wusu City	Chemical plant	1.21
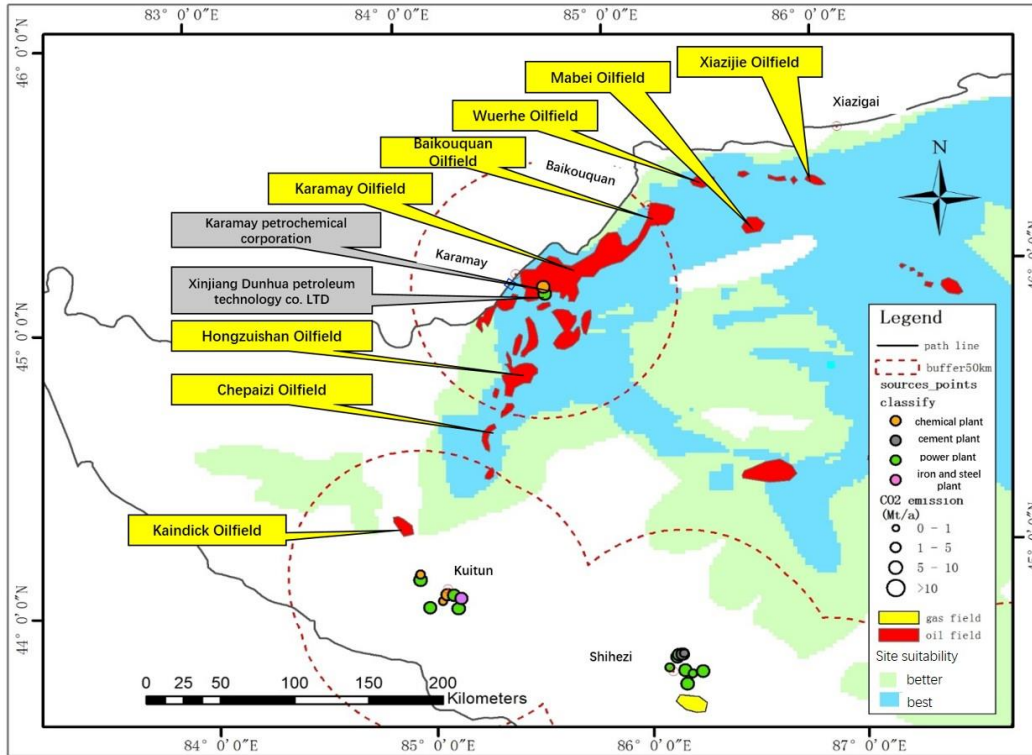
Figure 3.8 The location of oilfields and emission sources in Western Junngar Basin

3.2.2 THE EARLY DEMONSTRATION OPPORTUNITIES IN EASTERN JUNGGAR BASIN

Eastern Junggar Basin is suitable for CO_2-EWR demonstration projects. The main CO_2 emission points are chemical plants and power plants. The power plants are still not fully constructed. Once construction has been completed and the plants are put into operation, it is estimated that their annual emissions will be approximately 17.61 Mt/a. Guanghui New Energy Co., Ltd., which is a coal chemical plant, has CO_2 emissions of 14.58 Mt/a. More importantly, Guanghui New Energy has a strong willingness to reduce carbon emissions, and also has engaged in some related research. Furthermore, Ulungur Depression, located to the northwest of the Guanghui New Energy site, has large aquifer storage capacity and good geological conditions.

The Ulungur Depression is a first-level tectonic unit in the northeast edge of the Junggar Basin, with a diamond-shaped form. It covers an area of about 16,000 square kilometers, accounting for 13% of the basin's total area. The Ulungur Depression can be divided into two secondary tectonic units: the Hongyan step-fault zone and the Suosuoquan Depression from north to south, and is connected to the northern slope of the Luliang Uplift in the south. The current deposition thickness of the Suosuoquan Depression can reach 3,000 - 5,000 m. The large number of fault blocks, fault noses and lithologic structures formed during the Indo-China period and Yanshan period provide good traps.
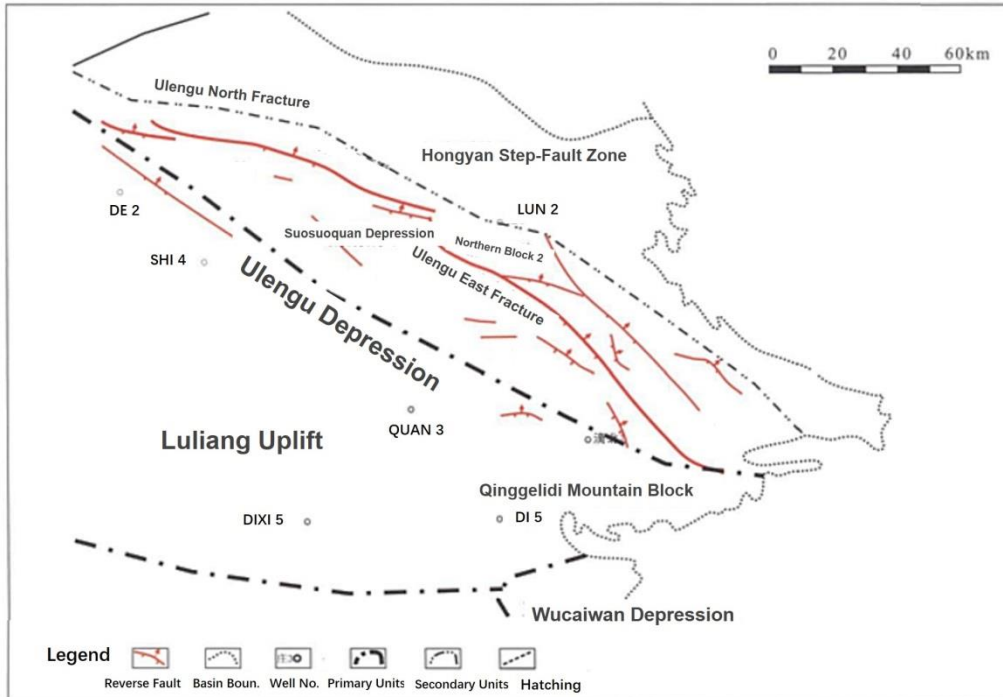
Figure 3.9 The main tectonics of Ulungur Depression in Eastern Junngar Basin

The Ulungur Depression has developed Carboniferous, Triassic, Jurassic, Cretaceous and Tertiary strata from bottom to top for, but lacks Permian strata. There are good reservoir conditions in the Depression. The sandstone of Jurassic Shishugou Group, Xishanyao Formation, Sangonghe Formation and Badaowan Formation has good physical properties. The huge thick mudstone between the upper Shishugou Group and lower Cretaceous system can serve as a regional caprock. The thickness of single layer mudstone is 10 - 100 m with an average thickness reaching 30 m. The huge thick mudstone below Xishanyao Formation can also serve as a regional caprock. The single layer thickness is 10 - 100 m with an average thickness reaching 20 m.
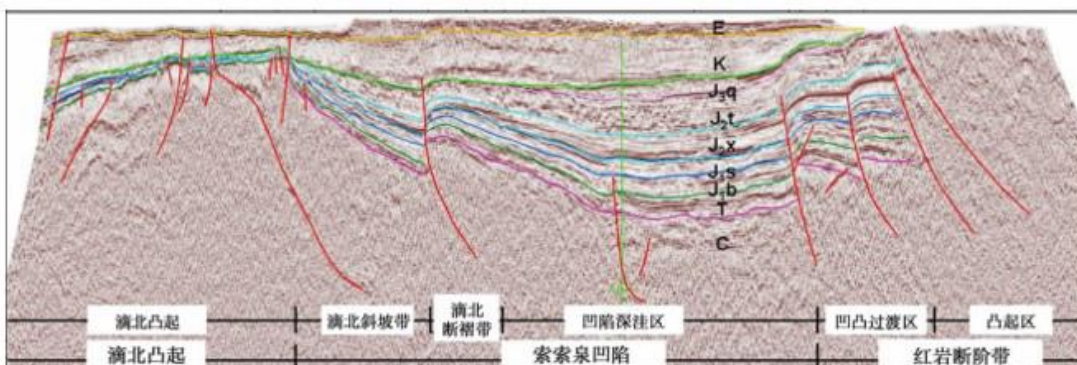

Figure 3.10 Seismic Section of Eastern Ulungur Depression (Mei Wenke, 2013)

Table 4.4 Jurassic Reservoir Caprock Assemblages of Ulungur Depression in Junggar Basin

Stratum	Lithologic Description	Reservoir cap

|	Qigu Formation	Mainly fuchsia and maroon mudstones, siltstone and coarse sandstone.	Caprock
Jurassic System	Toutunhe Formation	Sepia and grey mudstones, sandy mudstone, gray argillaceous sandstone, siltstone and fine sandstone are interbedded with different thickness.	Caprock
	Xishanyao Formation	The upper parts are grayish white pebbly sandstone. The lower parts are gray, grayish green and grayish black mudstones and siltstones.	Upper part reservoir, Lower part caprock
	Sangonghe Formation	The upper parts are grey mudstone, sandy mudstone mixed with siltstone, gray, grayish green, grayish black and tawny pebbly sandstones.	Upper part caprock, lower part reservoir
	Badaowan Formation	Gray and grayish green pebbly sandstones mixed with coal bed.	Reservoir
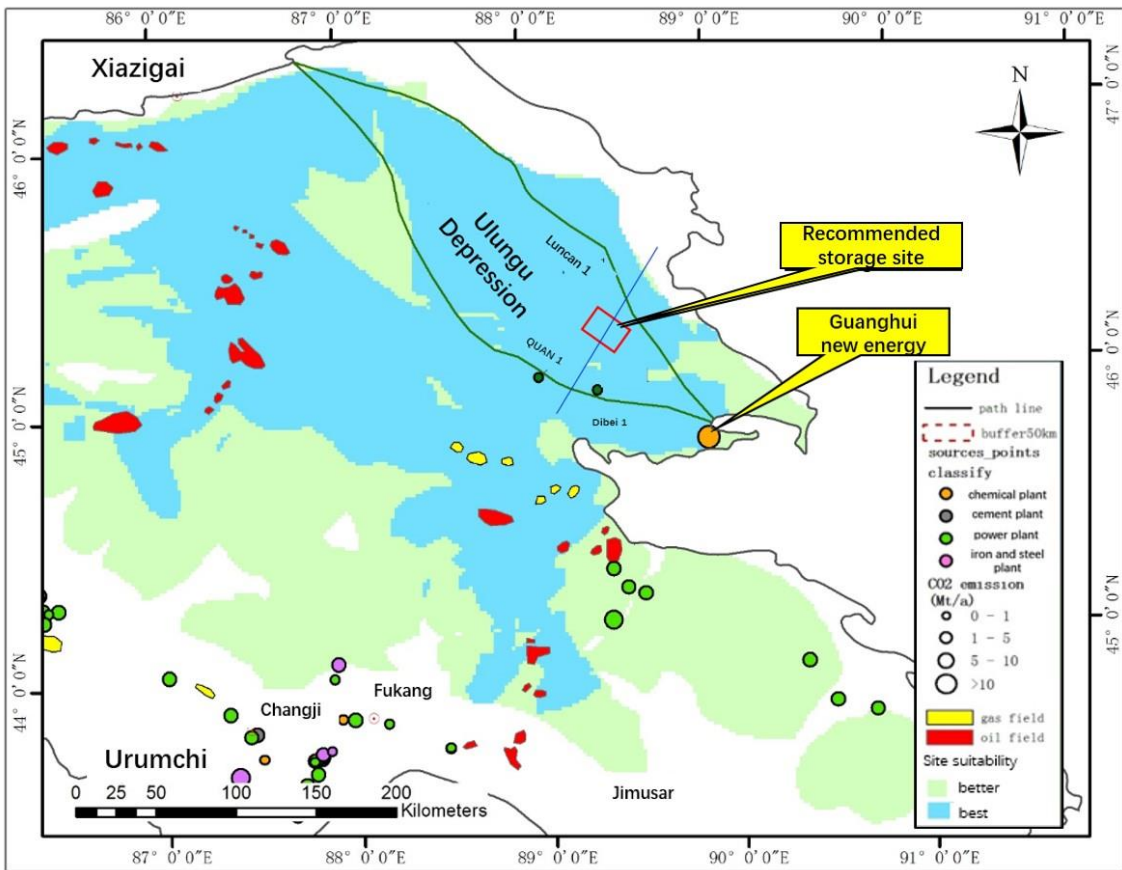
Figure 3.11 The CO$_2$-EWR early demonstration site in Eastern Junngar Basin

4. GEOLOGY OF STORAGE SITE FOR PRELIMINARY STUDY OF CO_2-EWR

4.1 REGIONAL GEOLOGY

The storage site for CO_2-EWR is mainly supported by the D7 well, which is an abandoned well completed by Sinopec in 2016. It is located in the south of Gurbantunggut Desert in the Junggar Basin, with no permanent settlements nearby, which could help us to carry out further geological investigation of the storage site and CO_2-EWR prefeasibility study.

The D7 well is located in the secondary tectonic unit of the Junggar Basin, Fukang Sag, with simple geostructure, stable crust, and almost no large historical earthquakes recorded in the surrounding area. Furthermore, few faults have developed in the target saline aquifers range from 800-3,500 m except for the lower Jurassic, and the D7 well is far away from the active faults developing in the Southern Basin.

Funded by the CAGS and China Geological Survey (CGS) project "Geological Survey of CO_2 Geological Storage in the Junggar and Other Typical Basins", data collection of drilling and logging, outcrops geological surveys, 2D seismic exploration, and downhole testing for reservoir characterisation and modeling were completed.

Figure 4.1 China Geological Survey area in the Junggar Basin

The D7 well drilling data shows that the strata in the storage site from old to young is as follows:

(1) Jurassic

Badaowan Formation, Sangonghe Formation, Xishanyao Formation, Toutunhe Formation, Qigu Formation;

(2) Cretaceous

Qingshuihe Formation, Hutubi Formation, Lianmuqin & Shengjinkou Formation, Donggou Formation.

(3) Tertiary

(4) Quaternary

Table 4.1 Stratigraphy of the D7 well

Strata				Label	Bottom /m	Thickness /m
Cenozoic	Neogene			N	1405.00	1405.00
	Paleogene			E	1945.50	540.50
Mesozoic	Cretaceous	Upper	Donggou	K_2d	2286.00	340.50
		Lower	Lianmuqin-Shengjinkou	K_1l+K_1s	2994.00	708.00
			Hutubi	K_1h	3595.50	601.50
			Qingshuihe	K_1q	3876.00	280.50
	Jurassic	Middle	Toutunhe	J_2t	4602.00	726.00
			Xishanyao	J_2x	4978.30	376.30
		Lower	Sangonghe	J_1s	5336.40	358.10
			Badaowan	J_1b	5405.00（not real bottom）	68.60

The Donggou Formation of the Cretaceous in the Eastern Junggar Basin has a total thickness of 356 m, mainly consisting of reddish-brown, purple-red mudstones and sandy mudstones with yellowish-gray siltstones and argillaceous siltstones. Among them, there is a set of thick muddy mudstones at the top of Donggou Formation, and there are sandstones, siltstones and argillaceous siltstones in the middle, upper and middle parts of Donggou Formation with different thickness.
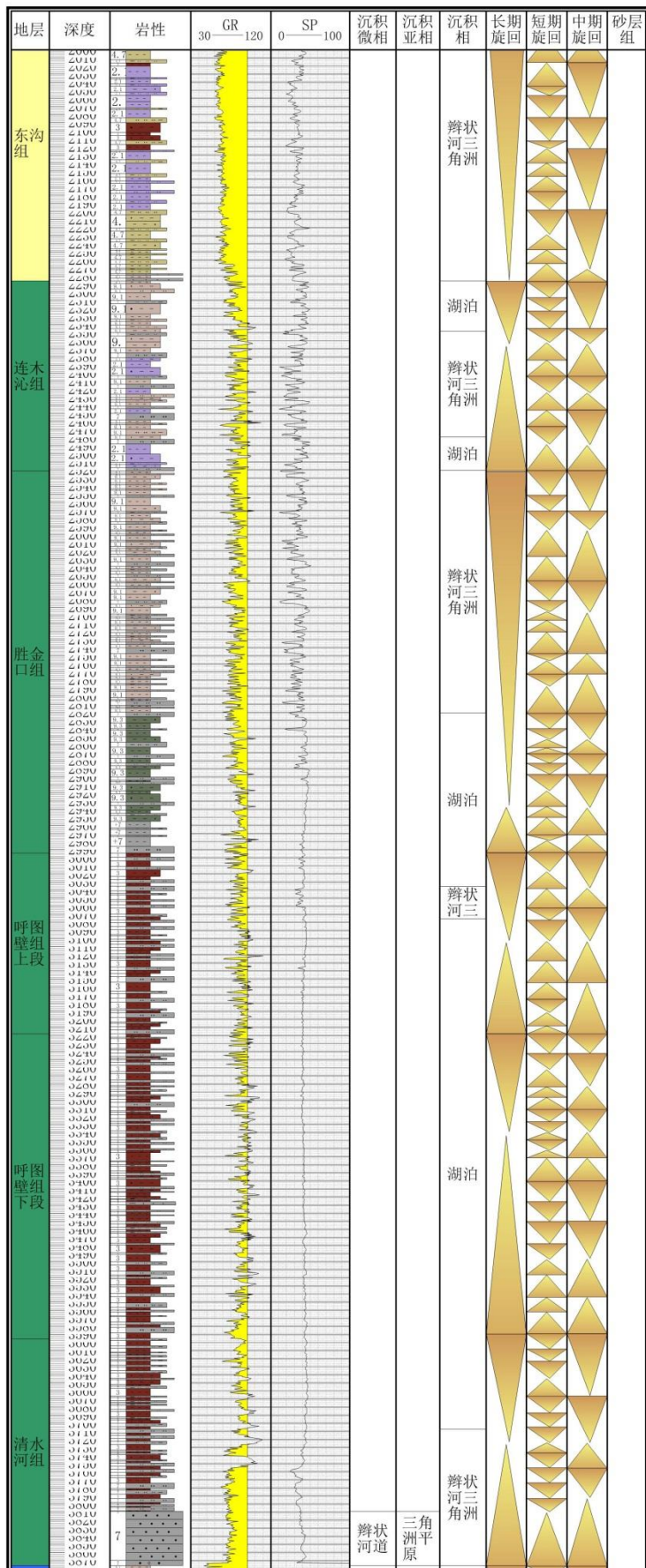
Figure 4.2 Cretaceous formations of the D7 well

4.2 RESERVOIR CHARACTERISATION

4.2.1 RESERVOIRS SELECTED FOR CO$_2$-EWR

Based on a geological study of drilling, logging and seismic exploration, we ultimately selected three sandstone saline aquifers to perforate as target reservoirs. The three perforated intervals are all sandstone aquifers, of which the first and second are developed in the Cretaceous Donggou Formation, and the third is developed in Lian-Sheng Formation. The geological information is shown in Table 4.2 and Figure 4.3.

Table 4.2 Reservoir characterisation of 3 perforated intervals

Interval	Formation	Depth /m	Average porosity /%	Average permeability /mD	Pressure /MPa	Temperature /℃
1st	Donggou	2038-2065	22.8	181.2	19	58.66
2nd	Donggou	2246.5-2265	23.8	209	22.1	66
3rd	Lian-Sheng	2392-2407	18.6	95.7	22.73	65.54
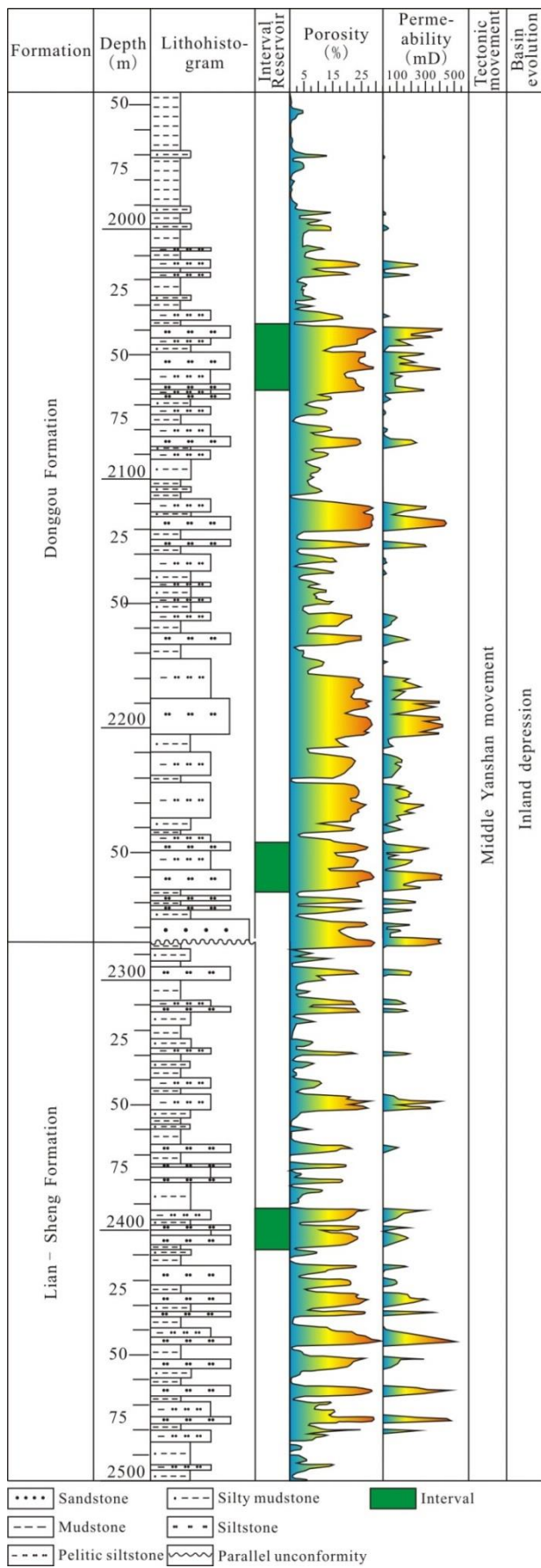
Figure 4.3 Stratigraphic histogram of 3 perforated intervals

4.2.2 Porosity and Permeability Prediction

(1) Logging

Based on the sequential stratigraphy correlation of the D7 well shown in Figure 4.2, we predicted the porosity and permeability using the logging data.

Figure 4.4 The relation curve of depth and porosity in the D7 well

In the figure the annotation reads $\phi=(5768.5-d)/18840$.

In the second figure the annotations read:
$$\kappa= (e^{\phi-4.728})^{1/3.308}, \phi>5\%$$
$$\kappa= e^{\phi-5.968}, \phi<=5\%$$

Figure 4.5 The relation curve of permeability and porosity in the D7 well
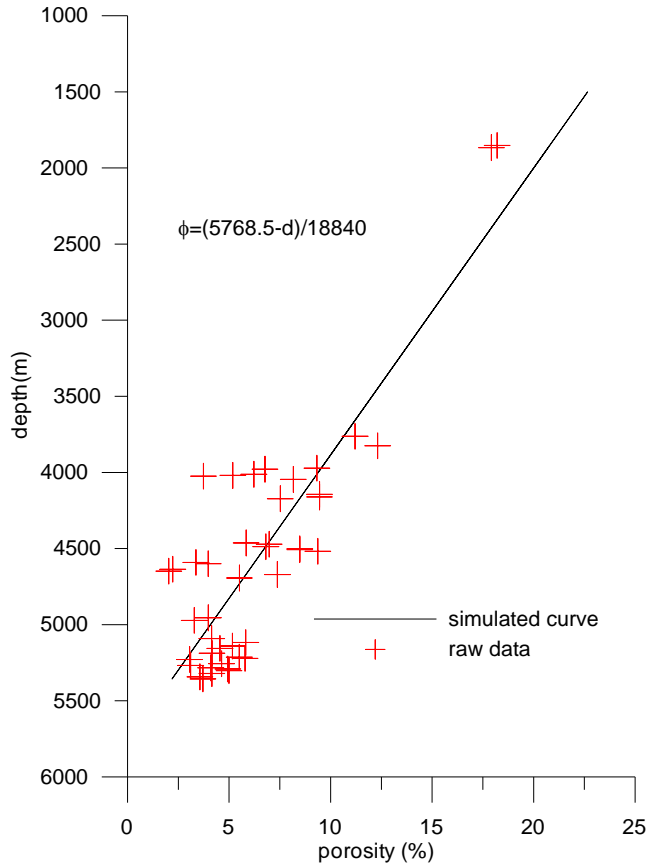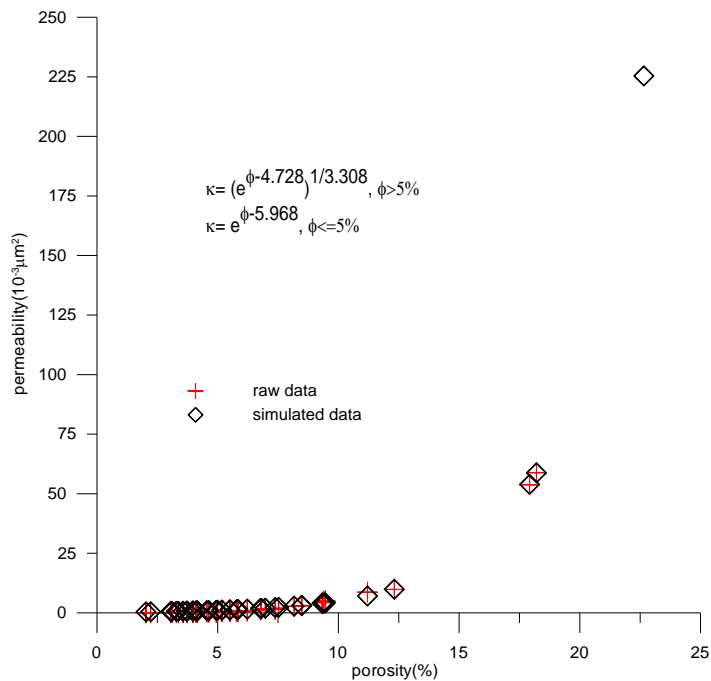
(2) 2D seismic

According to the preliminary analysis of the logging data of the D7 well storage site, rich groundwater has developed in the unconformity between the top of Jurassic and the bottom of Cretaceous, while a large thickness of lacustrine mudstone has developed in Hutubi Formation. Liansheng Formation and Shengjinkou Formation mainly consist of mudstones with thin sandstone layers of braided river delta sedimentary facies. The content of sandstone increases markedly, but the water quantity needs to be checked.

Therefore, in order to select the suitable and rich groundwater reservoirs, we carried out 2D seismic exploration (including 4 lines) around the D7 well covering an area of 10 km × 10 km. The results show that Cretaceousand Jurassic formations are characterised by gentle incline in a W-E direction with good continuity, undeveloped tectonic activity and no interlayer fractures.
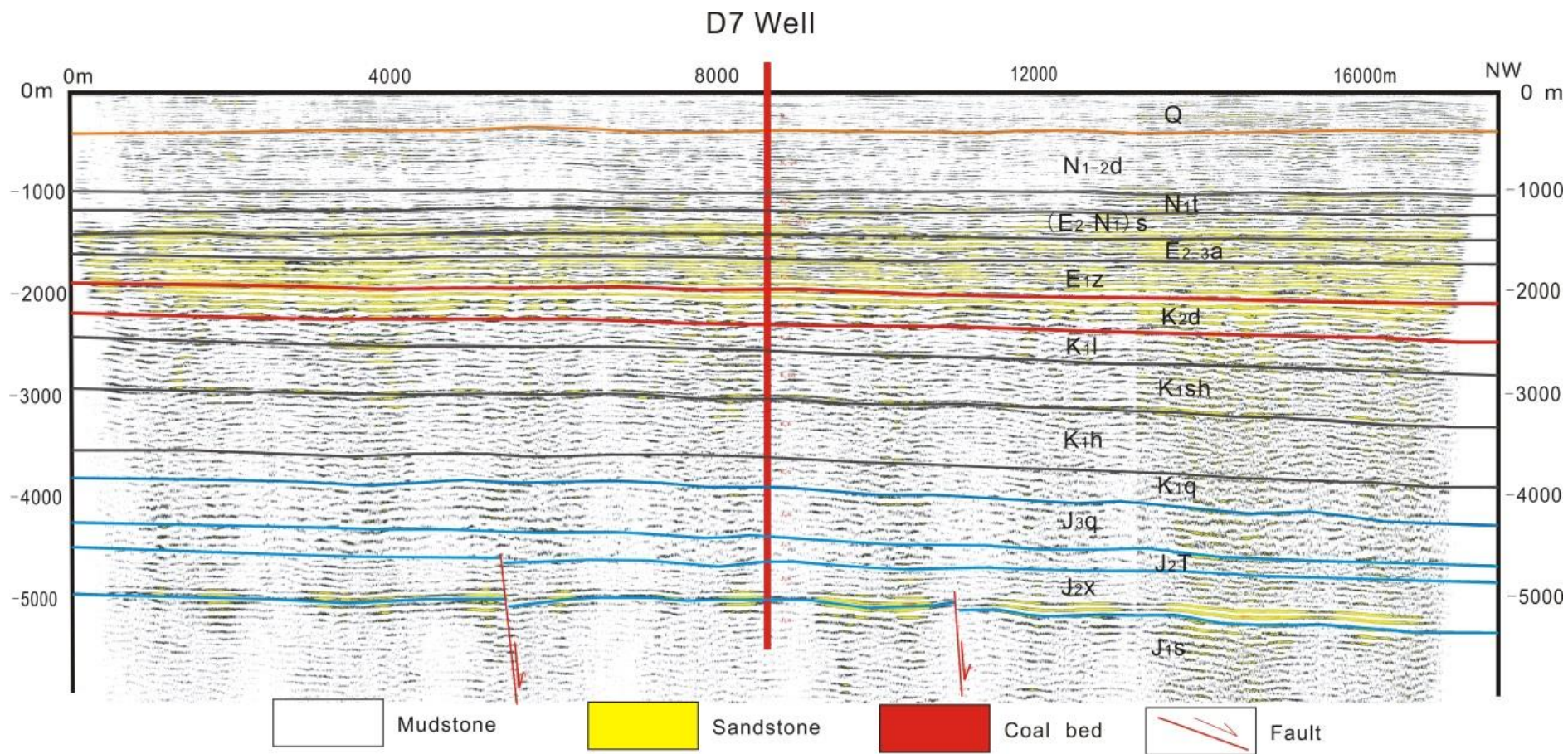
Figure 4.6 2D seismic profile of DZ01

(3) Downhole test

Funded by the CAGS and CGS project, we carried out reservoir tests in the D7 well. We selected three perforated layers to test the characteristics, and obtained key parameters based on the logging and 2D seismic exploration, as shown in Table 4.3 in detail.

Figure 4.7 Downhole reservoir test at the D7 site (by UAV)

Considering the drilling, logging, 2D seismic exploration and downhole test data, we inferred that the 2nd layer was the best saline aquifer suitable for preliminary study of CO_2-EWR of the three perforated layers. Furthermore, because of no good or continuous mudstone between the 1st and 2nd perforated layers, we considered the whole Donggou Formation as the potential reservoir for CO_2-EWR study.

Table 4.3 Selected and tested perforated layers

Perforated layer	Depth m	Thickness m	T ℃	P MPa	Pressure coefficient	Saline production m³/d	pH	TDS mg/L	Hydrochemistry	Well test permeability mD	Impact radius m
1	2038-2065	27	58.66	19	0.99	14	7.62	33404	CaCl2	1.68	55.5
2	2246.5-2265	18.5	66	22.1	1.0	41	7.51	40509	CaCl2	18.9	192
3	2392-2407	15	65.54	22.73	1.0	41	6.82	34453	CaCl2	7.47	138

4.3 3D GEOLOGICAL MODELING

Based on the 2D seismic amplitude data, we derived three main 2D seismic profiles which could be inputted into the grid model for static geological modeling, combined with the drilling and logging data of the D7 storage site.

Selecting the first and second aquifers of Donggou Formation as the target research reservoirs, a static model of Donggou Formation was finally set up in the range of 100 square kilometers with a total of 673,530 grids, and the size of each grid was 150 m × 150 m × 2.5 m. After upscaling of the grids in a vertical direction, there were 79 layers with a total of 338,910 grids, with the size of each grid being 150 m × 150 m × 5 m.
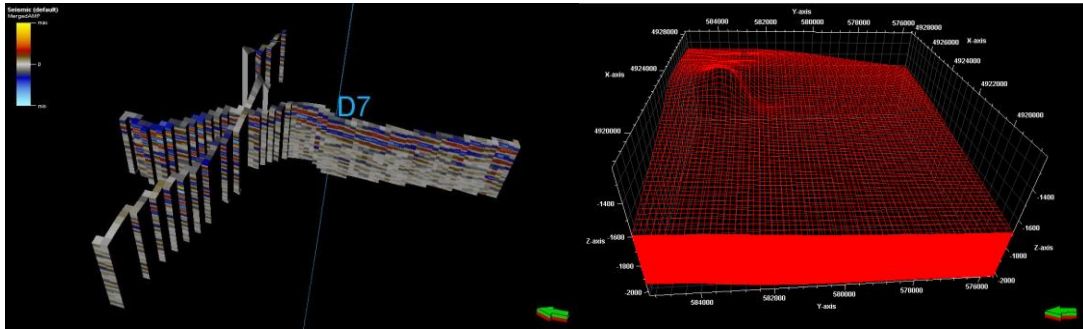

Figure 4.8 Seismic profiles and mesh generation of the geological model

Based on the drilling, logging and seismic amplitude data, we obtained a seismic amplitude model, shale content model (synergetic stochastic simulation with seismic amplitude model, with correlation coefficient of 0.545), porosity model (synergetic stochastic simulation with shale content model, with correlation coefficient of -0.968), and permeability model (synergetic stochastic simulation of permeability logarithm with porosity model, with correlation coefficient of 0.923). As shown in Figure 4.9, the permeability in the X and Y direction is the same, and the permeability in the Z direction is 0.3 times the permeability in the X direction.
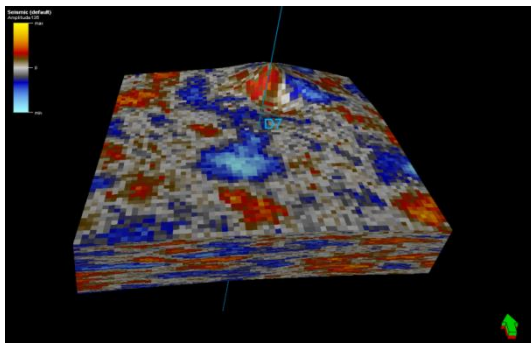
Seismic amplitude
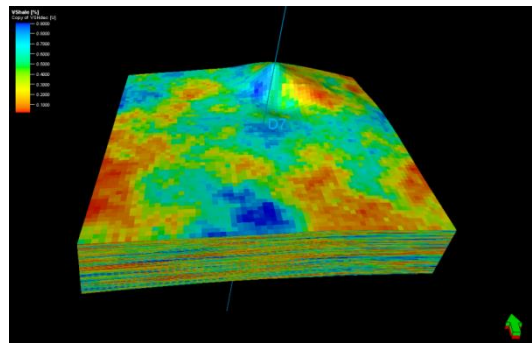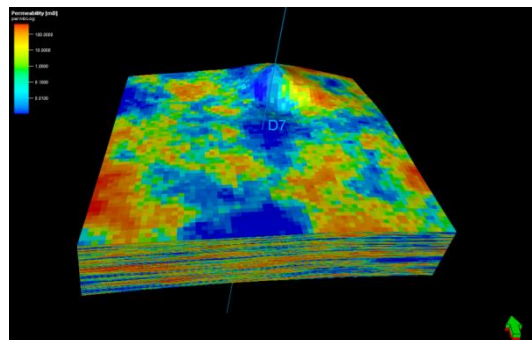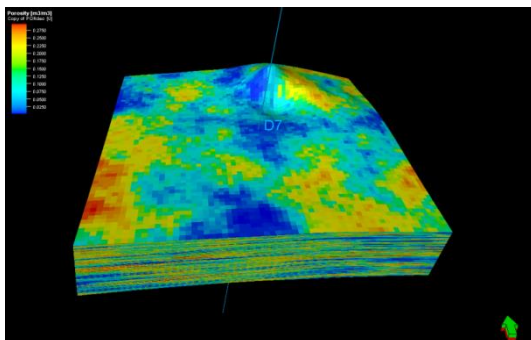
Shale content

Porosity   Permeability

Figure 4.9 Static geological model of seismic amplitude, shale content, porosity and permeability

In the geological model, the Donggou Formation ranges from -1481.40 m to -1821.88 m (altitude). The temperature in the centre of the model is 66℃, and the pressure is 20.6 MPa, with the formation pressure gradient ranging from 1.03 to 1.1 MPa / 100m and the fracture pressure gradient ranging from 1.63 to 2.25 MPa / 100m. The porosity of Donggou Formation ranges from 0.01 to 0.296, and the permeability ranges from 0.001 to 441mD.

4.4 ASSESSMENT OF CAPACITY AND GROUNDWATER RESOURCES

4.4.1 THEORETICAL CAPACITY ASSESSMENT

By using PETREL software, we assessed the total volume of rock to be 3.2551×10^{10} m^3, while the total volume of pores is 4.327×10^9 m^3, which could be regarded as the total theoretical groundwater resources volume.

Furthermore, based on the geological model, we evaluated the capacity of CO_2 storage by using the formula proposed by USDOE (2007) as mentioned in Section 2. The density of injected CO_2 underground is about 0.693g/cm^3 when the in-depth temperature is about 66℃ and the pressure is about 20.6 MPa.

The evaluated results show that, at a P50 level, the theoretical capacity of CO_2 geological storage in the D7 well storage site is 71.97 Mt.

Table 4.4 Capacity of CO_2 storage based on static reservoir modeling

	P$_{10}$	**P$_{50}$**	P$_{90}$
E_{saline} （Bachu, 2015）	1.2%	**2.4%**	4.1%
Total effective volume （m^3)	5.19E+07	**1.04E+08**	1.77E+08
Capacity (Mt）	35.98	**71.97**	122.94

4.4.2 CAPACITY ASSESSMENT BASED OF CO_2 INJECTION CASE STUDIES
(1) Cases

In order to evaluate the field scale capacity of CO_2 geological storage in the Donggou Formation, we hypothesised two cases with different CO_2 injection schemes for reservoir modeling as shown in Figure 4.10.

We defined the average temperature of the reservoir as 66℃, and set the pressure of the centre of the model at 20.6MPa, with formation pressure gradient ranging from 1.03 to 1.1 MPa per 100 m and the fracture pressure gradient ranging from 1.63 to 2.25 MPa per 100 m.
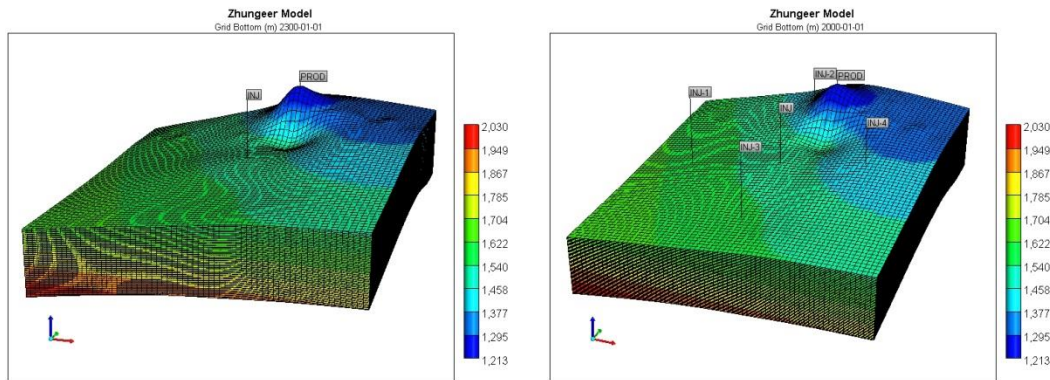
Figure 4.10 Two cases with different injection schemes (Case 1 is on the left and Case 2 is on the right)

Based on the static geological model, the formation parameters were inputted into the injection modelling, as shown in Figure 4.11. The two typical injection cases were as follows:

Case 1: One injection well and one production well nearby. Simulation time of 300 years. The injection well is the Dong 7 well. The perforation location is mainly in the middle and lower part. The maximum allowable injection pressure at the bottom of the well is less than 50 MPa (stop injection when injection pressure exceeds 50 MPa). The CO_2 injection rate is set at 500,000 tons per year for a continuous period of 50 years, followed by a simulation of 250 years. The production well is set at the top of the Donggou Formation with the maximum allowable pressure of 50 MPa at the bottom of the well.

Case 2: Five injection wells, one production well, simulated for 300 years. Dong 7 well is located at the centre of the model, and the distance between the injection wells is 3 km. The perforating location is mainly in the middle and lower part of Donggou Formation.
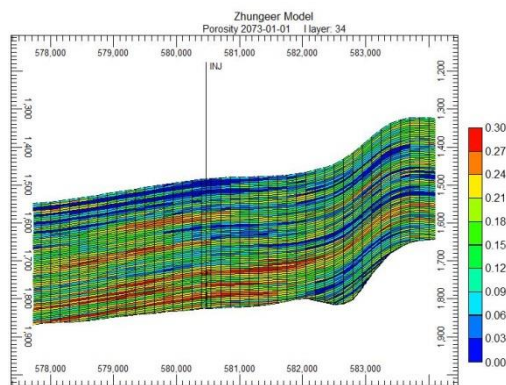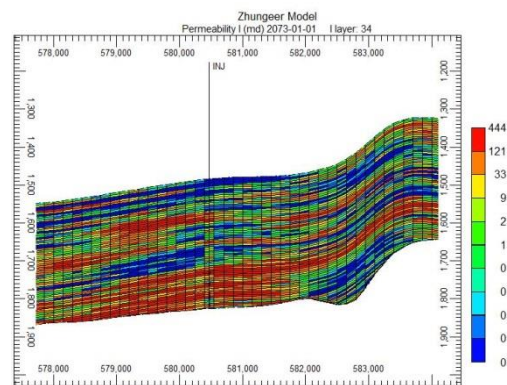
Porosity   Permeability in horizontal direction

38

Permeability in vertical direction   Pressure
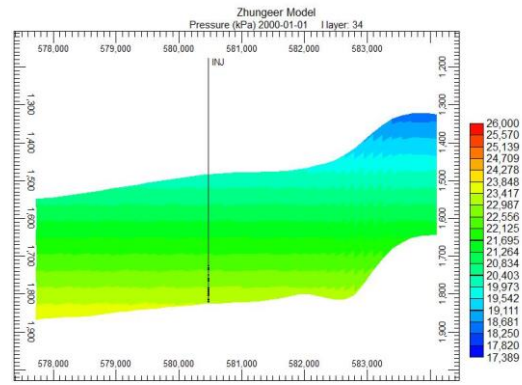
Fig. 4.11 Numerical models for the case studies

The allowable bottom injection pressure must be less than 50MPa (stop injection when injection pressure exceeds 50 MPa), and the annual injection amount is 500,000 tons for a continuous period of 50 years, followed by a simulation of 250 years. The production well is set at the top of the Donggou Formation with the maximum allowable pressure of 50 MPa at the bottom of the well.
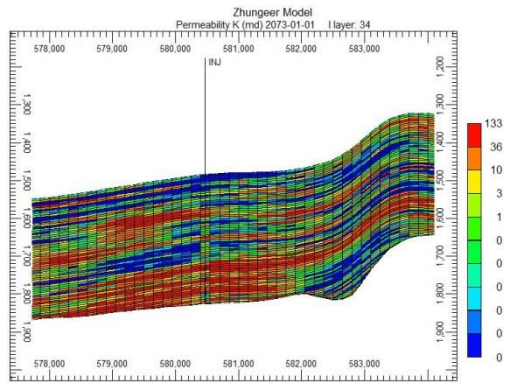
(2) Capacity

In the Case 1 and Case 2 models, CO_2 was supposed to be continuously injected for 50 years at an injection volume of 2 million tons a year for a cumulative total of 1.919×10^{12} mole (84.41×10^6 tons). As shown in Figure 4.12, the injected CO_2 will be mainly trapped as gas CO_2 and dissolved CO_2. During the CO_2 injection, both the amount of gas and dissolution trapped CO_2 increase, but the amount of gas trapping is much larger. However, after injection completion, the total amount of dissolved CO_2 increases while the gas CO_2 decreases.

After 300 years, the total amount of trapped CO_2 including residual and dissolution trapping is about 7.059×10^{11} mole (about 31.063×10^6 t) in Case 1 and 8.653×10^{11} mole (about 38.077×10^6 t) in Case 2.
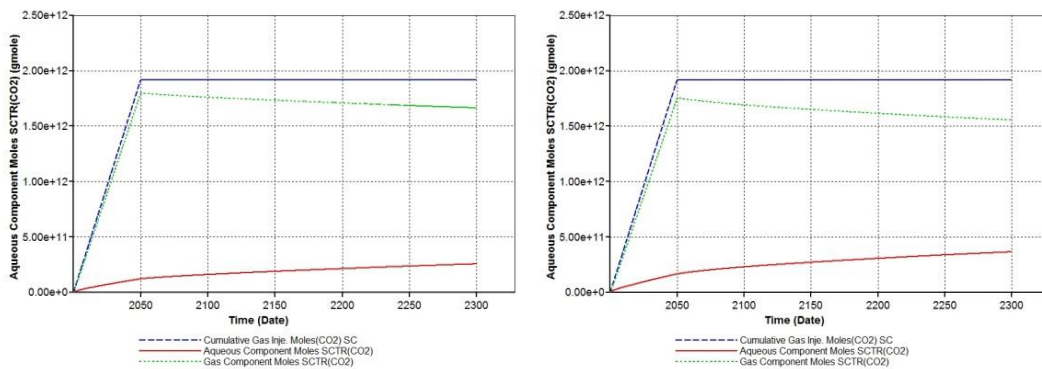
Figure 4.11 Gas CO_2 and dissolved CO_2 of the two case studies
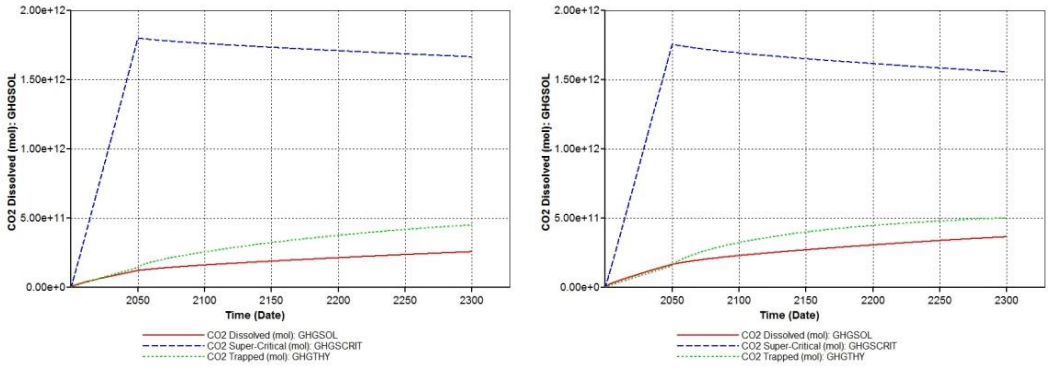
Figure 4.12 Total amount of trapped CO$_2$ of the two case studies

(3) Pressure

During the CO$_2$ injection, the pressure in the reservoir will increase. In Case 1 and Case 2, the overall average reservoir pressure increases to 39.776 MPa and 39.615 MPa respectively from the initial 21.878 MPa (or 81.81% and 81.07% respectively).
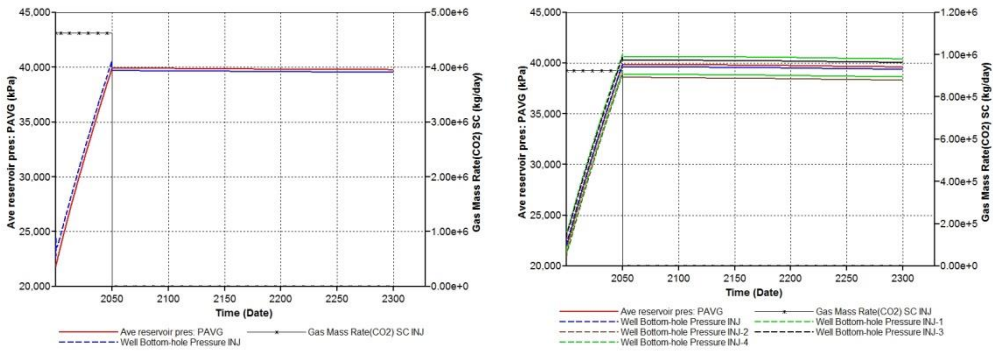
Figure 4.13 Pressure in the reservoir and bottom of injection well of the two case studies

(4) CO$_2$ distribution

As shown in the Figure 4.14, the CO$_2$ migration distance is about 3,500 m in a N-E direction in Case 1, and the distance upwards is about 300 m. In Case 2, the CO$_2$ plume is much larger than Case 1 because of more injection wells.
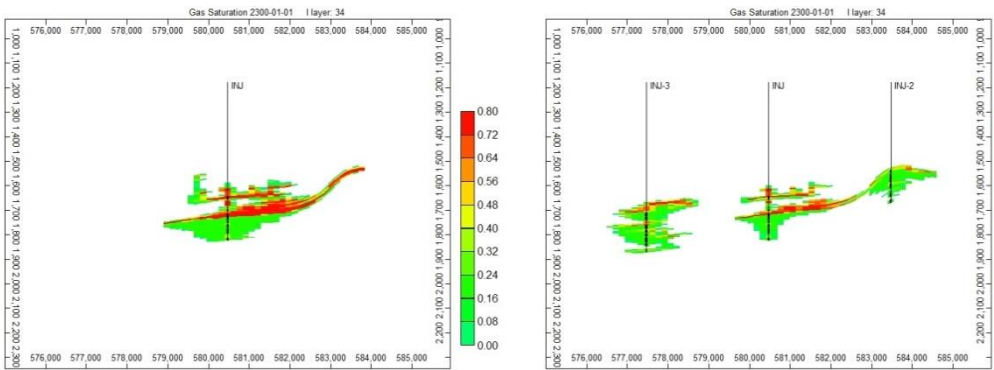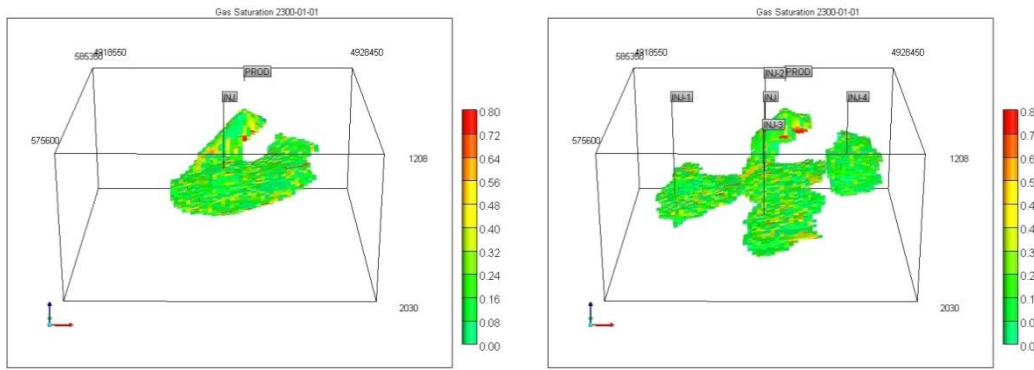
Figure 4.14 CO₂ distribution after 300 years of Case 1 and Case 2

(5) CO₂ trapping

The numerical simulation results of dissolution trapped CO_2 are shown in Figure 4.15. The dissolved CO_2 plume near the injection well is completely connected, with a maximum distribution of 8.6 km north to south, 9.3 km east to west, and a maximum vertical thickness close to 300 m. The residual trapped CO_2 distribution is similar to the dissolution trapping, as shown in Figure 4.16.
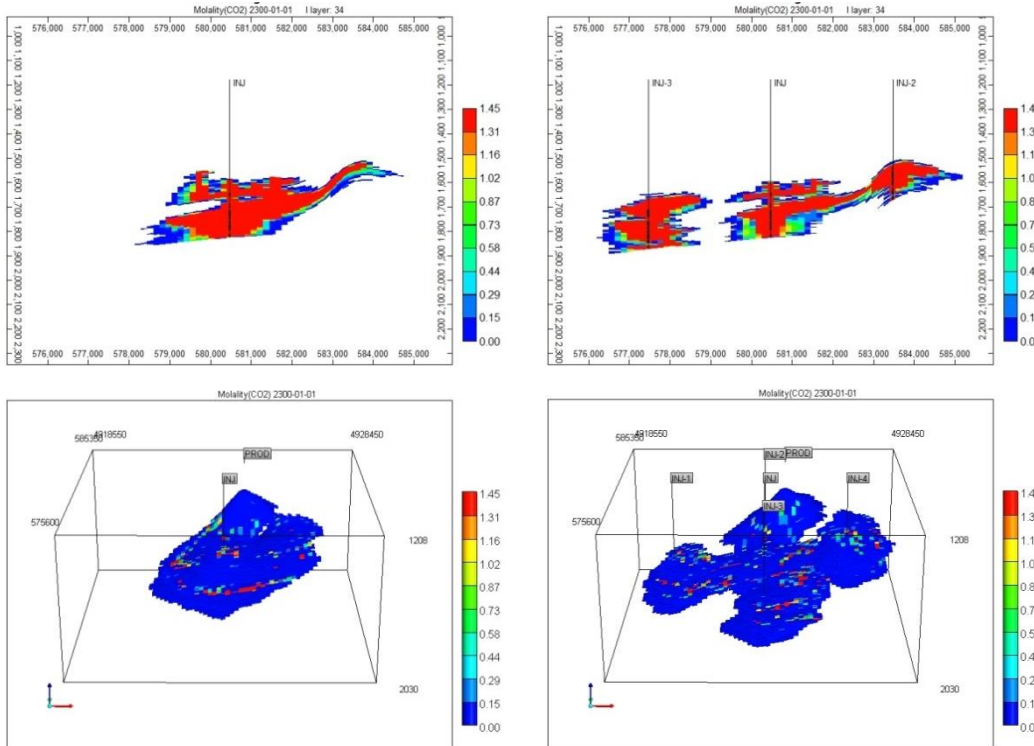
Figure 4.15 Dissolved CO₂ distribution after 300 years of Case 1 and Case 2
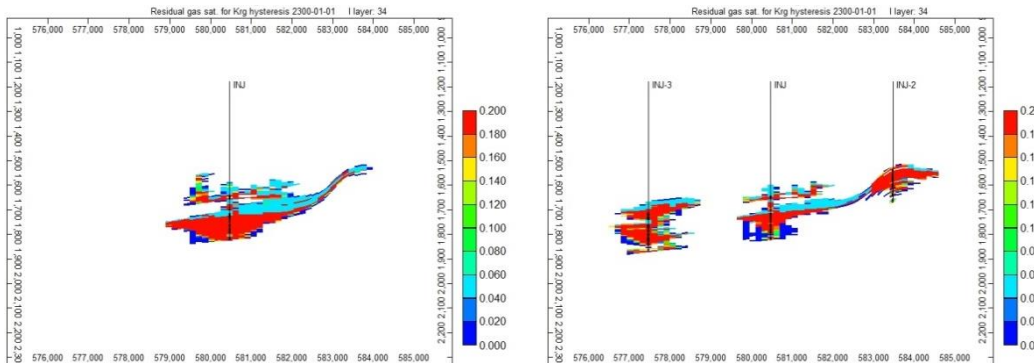
Figure 4.16 Residual trapped CO$_2$ distribution after 300 years of Case 1 and Case 2

As shown in Table 4.5, we can infer that more injection wells could enhance the effectiveness of CO$_2$ storage and enlarge the area of CO$_2$ distribution, which could also enhance the security of CO$_2$ storage. However, more injection wells also means higher cost.

Table 4.5 Total amount of injected CO$_2$ and trapping

CO$_2$ Storage Amounts in Reservoir	Case	Million tonne	kg	Moles	Percentage %
Total injection		84.414	8.441E+10	1.919E+12	100.00%
Supercritical gas		73.234	7.32E+10	1.664E+12	86.76%
Residual trapping gas	Case1	19.813	1.98E+10	4.502E+11	23.47%
Dissolved gas in water		11.250	1.125E+10	2.557E+11	13.33%
Total trapping gas		31.063	3.11E+10	7.059E+11	36.80%
Total injection		84.414	8.441E+10	1.919E+12	100.00%
Supercritical gas		68.437	6.84E+10	1.555E+12	81.07%
Residual trapping gas	Case2	22.063	2.21E+10	5.013E+11	26.14%
Dissolved gas in water		16.013	1.601E+10	3.639E+11	18.97%
Total trapping gas		38.077	3.81E+10	8.653E+11	45.11%

5. NUMERICAL SIMULATION OF CO_2-EWR IN THE D7 WELL SITE

In China, the Junggar Basin, with huge carbon emissions and deep saline aquifers having good geology, has the greatest early opportunities for CO_2-EWR or storage. The objective of our research is to evaluate the enhanced efficiency of CO_2 storage and saline production, including total CO_2 injection and saline production when CO_2 breaks through into the production well, based on the reservoir characterisation and modeling using the China Geological Survey (CGS) future CO_2-EWR test site in the Eastern Junggar Basin as a case study. The CGS CO_2-EWR site is located in Fukang Sag of the Junggar Basin, which has gentle formations and a dip angle of about 5 degrees from southwest to northeast. Currently, there has been one deep hole in the site for CO_2-EWR prefeasibility study. Three intervals are perforated between the depths of 1,945.5-2,994 m without faults.

5.1 ENHANCED EFFICIENCY OF CO_2 STORAGE AND SALINE PRODUCTION

5.1.1 UPSCALING

Based on the reservoir characterisation and geological model, we obtained the upscaling model for numerical simulation of CO_2-EWR. The new model is generalised into homogeneous isotropic and infinitely extended sandstone formations using irregular mesh generation.

Assuming that the spacing between injection and production wells is 2 km, in order to avoid the boundary impact, the X and Y directions are set to 20 km, and each layer is divided into 1,297 grids. The accuracy of porosity and permeability for each sample point in the original logging data is 0.125 m, and we obtained the porosity and permeability of the three perforated layers by taking the weighted mean values of each of the 10 logging points. The subdivision accuracy of each layer in the Z direction is 1.25 m, and the number of vertical grids of each sub-reservoir is different according to the reservoir thickness. The first sub-reservoir is vertically divided into 16 layers, with 20,752 grids; the second sub-reservoir is vertically divided into 18 layers, with 23,346 grids; the third sub-reservoir is vertically divided into 15 layers, with 19,455 grids.
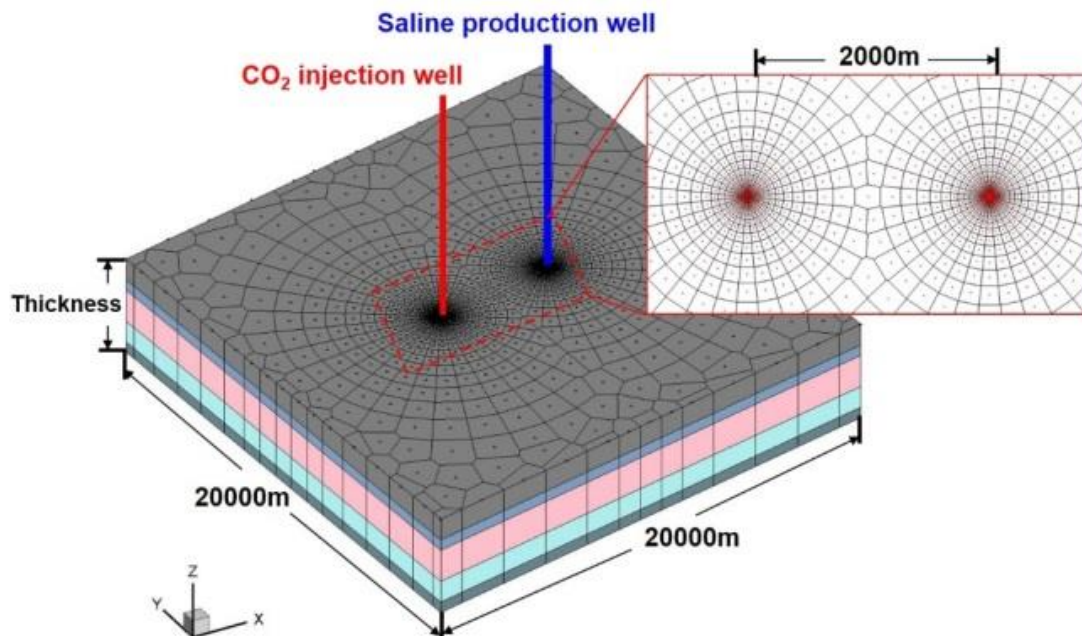

Figure 5.1 Mesh model of field scale CO_2-EWR test site (X: 20km; Y: 20km)

5.1.2 SIMULATED CONDITIONS AND KEY PARAMETERS

We used TOUGH2 (Transport of Unsaturated Groundwater and Heat) software to simulate the CO_2-EWR in the D7 storage site.

The reservoir formula modeling based on Darcy's law is as follows:

$$\frac{d}{dt}\int_{V_n} A^\kappa dV = \int_{\Gamma_n} \mathbf{F}^\kappa \cdot \mathbf{n}\, d\Gamma + \int_{V_n} q^\kappa dV \qquad (5\text{-}1)$$

Where V_n is the volume; Γ_n is area; κ is the component of fluid, κ=1，2，3，…; A^κ is the mass term of κ; F^κ is the mass exchange; q^κ is the source sink term; n is the unit normal vector; t is time。

To simulate the enhanced efficiency of CO_2 storage and saline production, the given conditions of the push-pull test for numerical simulation are as follows:

(1) Assume that there will be a water production well and the distance between the CO_2 injection well and production well is 2 km;

(2) Simulate the cases of CO_2-EWR push-pull test in different reservoirs separately;

(3) Specify a constant injection pressure at the wellhead of 7 MPa to inject CO_2, and 0.3 times the reservoir pressure to produce saline;

(4) Boundary condition: the lateral boundaries are defined with Dirichlet boundary conditions, and the upper boundary of the reservoir is assumed to be an impermeable boundary, as is the bottom boundary;

(5) The temperature and pressure conditions of each layer in the model are in-depth values, and the isothermal model is used in the simulation study.

5.1.3 RESULTS

(1) CO_2 migration in reservoirs

The results show that, for the distance of 2 km between injection well and production well, there are differences in the time of CO_2 breakthrough to the saline production well in the three reservoirs: the 1st reservoir is 5.67 years, the 2nd reservoir is 3.86 years, and the 3rd reservoir is 3.18 years. The CO_2 spatial distribution by using CO_2 storage only and CO_2-EWR, at the time of CO_2 breakthrough, is shown in Figure 5.2.
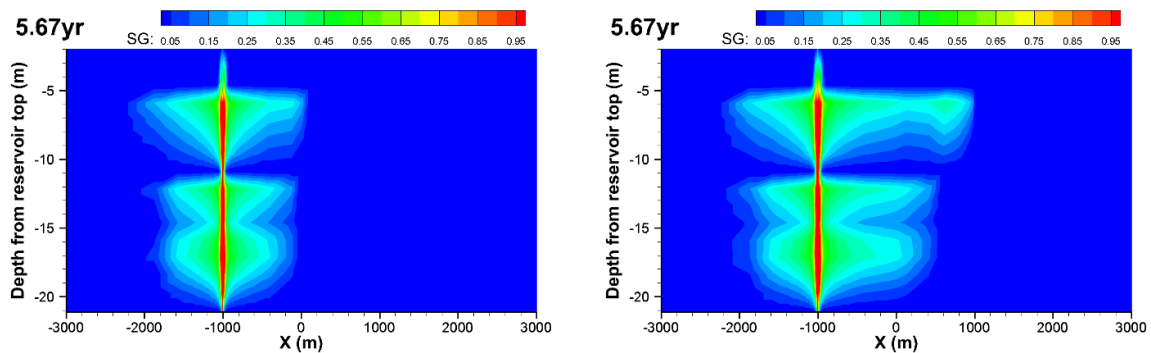
a. Only CO_2 storage in the 1st reservoir   b. CO_2-EWR in the 1st reservoir
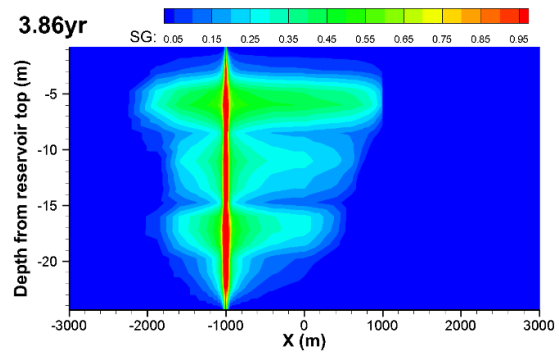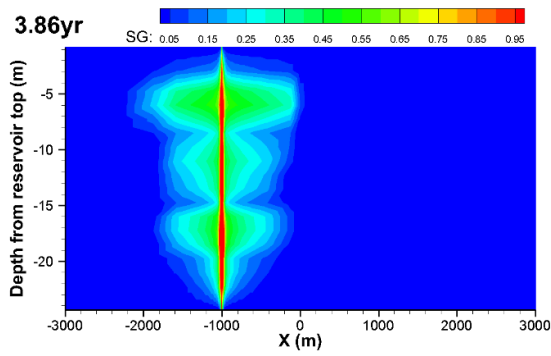
c. Only CO_2 storage in the 2nd reservoir   d. CO_2-EWR in the 2nd reservoir
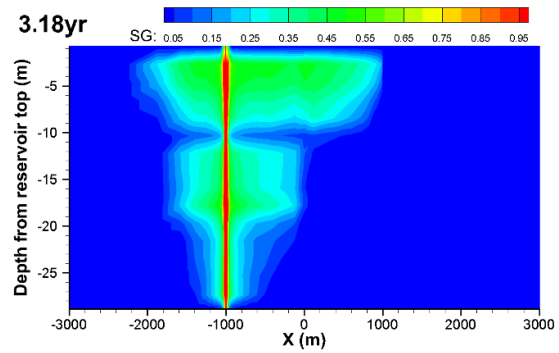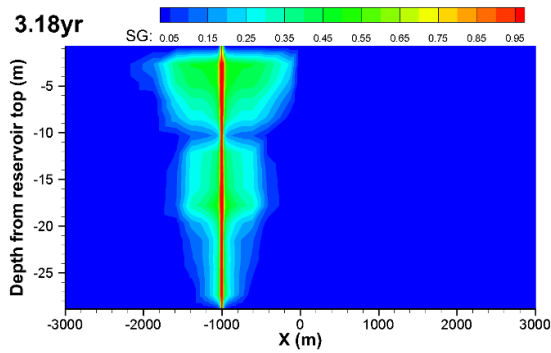
e. Only CO_2 storage in the 3rd reservoir   f. CO_2-EWR in the 3rd reservoir

Figure 5.2 CO_2 injection rates change with time in different reservoirs

Table 5.1 Results of numerical simulation

Reservoirs		1st	2nd	3rd
CO_2 migration distance		900 m	950 m	980 m
Total CO_2 injection	Only CO_2 storage	1.55 Mt, and 273 kt/a	2.22 Mt, and 576 kt	2.30 Mt, and 723 kt
	CO_2-EWR	2.35 Mt, and 414 kt/a	3.67 Mt, and 952 kt/a	3.71 Mt, and 1.17 Mt/a
	Enhanced efficiency	51.68%	65.33%	61.18%
Total saline production	Only saline production	4.31 Mt, and 759 kt/a	7.08 Mt, and 1.84 Mt/a	6.67 Mt, and 2.1 Mt/a
	CO_2-EWR	4.61 Mt, and 812 kt/a	7.60 Mt, and 1.97 Mt/a	7.17 Mt, and 2.25 Mt/a

	Enhanced efficiency	7.00%	7.30%	7.48%

(2) Enhanced efficiency

The results of enhanced efficiency of CO_2 storage and saline production, and the total amount of CO_2 injection and saline production, are shown in Table 5.1. From the simulated results we can infer that CO_2-EWR could greatly improve the total amount of CO_2 injection and saline production.

(1) 1st reservoir

If using the standalone CO_2 geological storage technology, CO_2 migration distance is 900m, and the total amount of injected CO_2 is 1.55 million tons after 5.67 years, with an annual average injection rate of 273 kilotons per year; if using saline production technology only, the total amount of saline produced is 4.31 million tons with an annual average production rate of 759 kilotons per year.

However, if using CO_2-EWR technology, when the injected CO_2 breaks through into the saline production well, the total amount of injected CO_2 is 2.35 million tons with an annual average injection rate of 414 kilotons, and the total amount of produced saline is 4.61 million tons with an annual average injection rate of 812 kilotons per year. Compared with the standalone CO_2 geological storage technology and saline production, the CO_2-EWR technology has increased the CO_2 storage capacity by 51.68% and the saline production by 7%.

(2) 2nd reservoir

If using the standalone CO_2 geological storage technology, CO_2 migration distance is 950 m, and the total amount of injected CO_2 is 2.22 million tons after 3.86 years with an annual average injection rate of 576 kilotons per year; if using saline production technology only, the total amount of saline produced is 7.08 million tons with an annual average production rate of 1.84 million tons per year.

However, if using CO_2-EWR technology, when the injected CO_2 breaks through into the saline production well, the total amount of injected CO_2 is 3.67 million tons with an annual average injection rate of 952 kilotons, and the total amount of produced saline is 7.60 million tons with an annual average injection rate of 1.97 million tons per year. Compared with the standalone CO_2 geological storage technology and saline production, the CO_2-EWR technology has increased the CO_2 storage capacity by 65.33% and the saline production by 7.3%.

(3) 3rd reservoir

If using the standalone CO_2 geological storage technology, CO_2 migration distance is 980 m, and the total amount of injected CO_2 is 2.30 million tons after 3.18 years with an annual average injection rate of 723 kilotons per year; if using saline production technology only, the total amount of saline produced is 6.67 million tons with an annual average production rate of 2.10 million tons per year.

However, if using CO_2-EWR technology, when the injected CO_2 breaks through into the saline production well, the total amount of injected CO_2 is 3.71 million tons with an annual average injection rate of 1.17 million tons and the total amount of produced saline is 7.17 million tons with an annual average injection rate of 2.25 million tons per year. Compared with the standalone CO_2 geological storage technology and saline production, the CO_2-EWR technology has increased the CO_2 storage capacity by 61.18% and the saline production by 7.48%.

5.2 SINGLE WELL RESIDUAL AND DISSOLUTION TRAPPING TEST PLAN

Considering the engineering conditions of the D7 storage site, we selected the 2nd perforated layer with better geological conditions than the other two layers, and proposed a preliminary single well residual and dissolution trapping test plan as follows:

(1) First stage:

Pull enough formation liquid and test the reservoir permeability;

Cases: pull saline 100-1,000 m^3

Close the hole (until the pressure recovers);

Inject the formation liquid back into reservoirs, test pressure response.

Close the hole (until the pressure recovers);

(2) Second stage:

Inject CO_2 into the reservoirs, test the pressure response and reservoir injectivity;

Cases：100t - 1,000t

Close the hole;

(3) Third stage: mass formation liquid production

Pull back the liquid including CO_2 and saline, to test the pressure response and tracers, CO_2 and water quality.

Cases: about 2 times the amount of CO_2 injection.

Final disposal.

In our research, we used the TOUGH2/ECO2N computer program to study the prefeasibility of CO2-EWR.

5.2.1 SIMULATION MODEL

(1) Geometric model

In the upscaling model, the 2nd perforated layer is 18.5 m thick, extending homogenously in horizontal direction. In the vertical direction, there are 18 layers; in the horizontal direction, there are 50 grids within the range of 10 km. The final geological model is shown in Figure 5.3 (A).

注入井　　　　$R_{max}=10000$ m

R

砂岩储层

18.5m

地表　　注入井

2246.5m

18.5m

非渗透盖层

CO_2羽

砂岩地层　　注入点
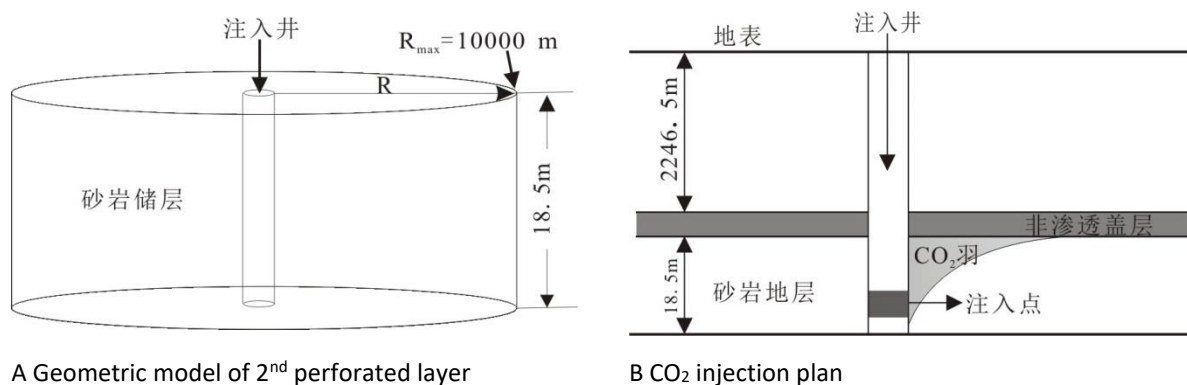
A Geometric model of 2nd perforated layer　　　　B CO_2 injection plan

Fig. 5.3 Conceptual model of single well test simulation

(2) Key parameters of the reservoir

Based on the geology of the D7 well storage site, we upscaled the 2nd perforated layer, which is homogenous in the horizontal direction, and the key parameters are shown in Table 5.2.

Table 5.2 Key parameters of the reservoir

Key parameters	Value	Other parameters	Value
Thickness (m)	18.5	**1. Relative permeability model**	
Permeability (×10⁻³μm²)	Heterogenous	Liquid (van Genuchten, 1980)：	
Porosity (%)	Heterogenous	$k_{rl} = \sqrt{S^*}\left\{1-(1-\left[S^*\right]^{1/m})^m\right\}^2$	$S^* = (S_l - S_{lr})/(1-S_{lr})$
Pore compression coefficient (Pa⁻¹)	4.5×10^{-10}		
Rock density (kg/m³)	2600	S_{lr}： Residual water saturation	S_{lr} =0.30
Coefficient of heat conduction (W/m °C)	2.51	m： index	m=0.457
Specific heat of rock (J/kg °C)	920	Gas (Corey, 1954)：	
Temperature (°C)	63	$k_{rg} = (1-\hat{S})^2(1-\hat{S}^2)$	$\hat{S} = (S_l - S_{lr})/(S_l - S_{lr} - S_{gr})$
Pressure (kPa)	Reservoir hydrostatic pressure	S_{gr}： Residual gas saturation	S_{gr}=0.05
Salinity (wt.-%)		**2. Capillary pressure van Genuchten (1980)：**	
	4.3	$P_{cap} = -P_0(\left[S^*\right]^{-1/m}-1)^{1-m}$	$S^* = (S_l - S_{lr})/(1-S_{lr})$
		S_{lr}： Residual water saturation	S_{lr}=0
		m： index	m=0.457
		P_0： Capillary entry pressure	P_0=19.61kPa

5.2.2 RESULTS

(1) First stage

The first stage (case): saline pull of 1,000 m^3 for 25 days with constant flow (40m^3/d). The pressure change characteristics in the reservoir during the saline pull are shown in Figure 5.4.
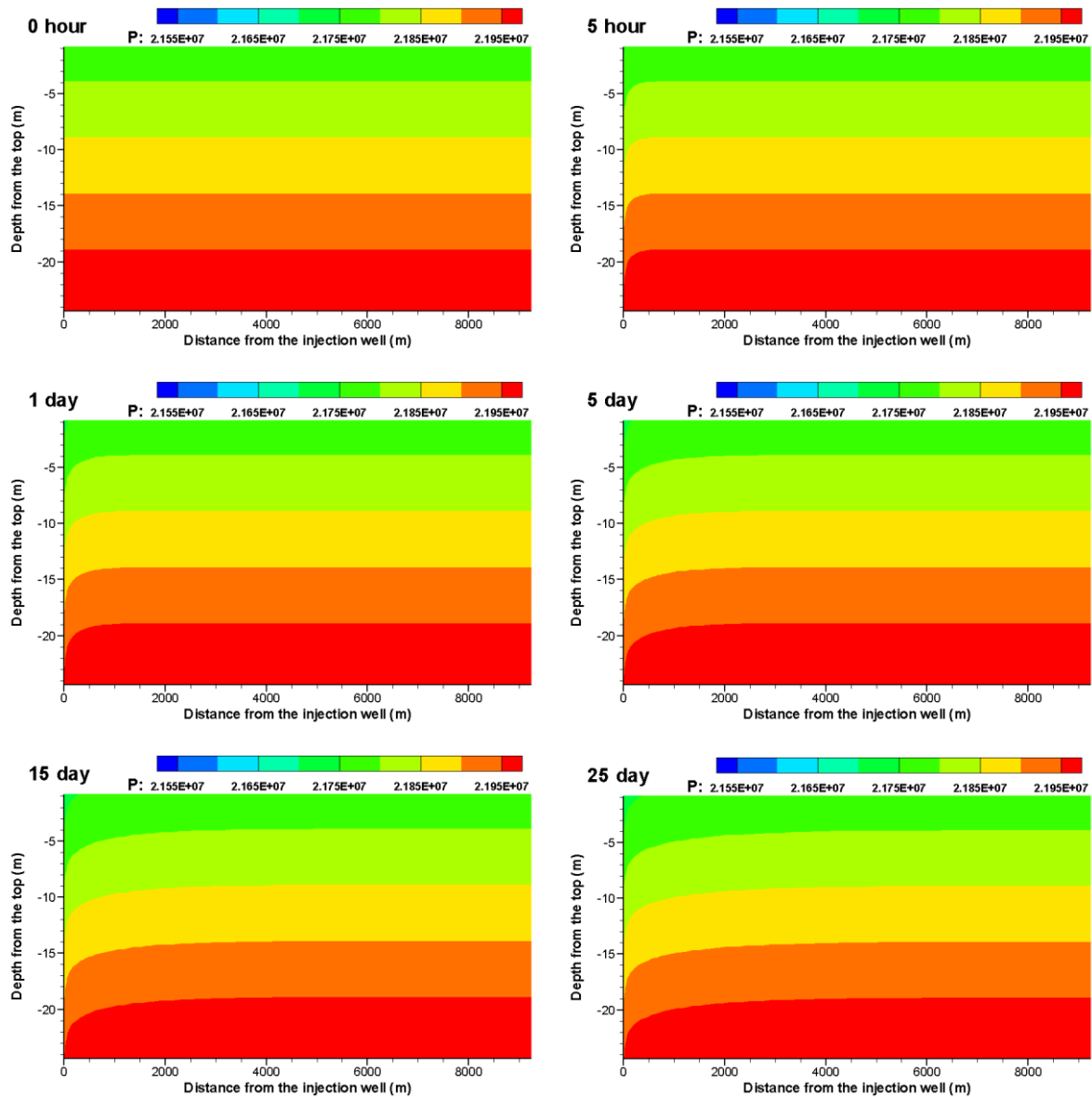
Figure 5.4 The pressure change during the saline production with constant flow

During the pressure recovery stage, the pressure recovered to its original pressure 150 days after saline production stopped. The pressure change characteristics are shown in Figure 5.5.
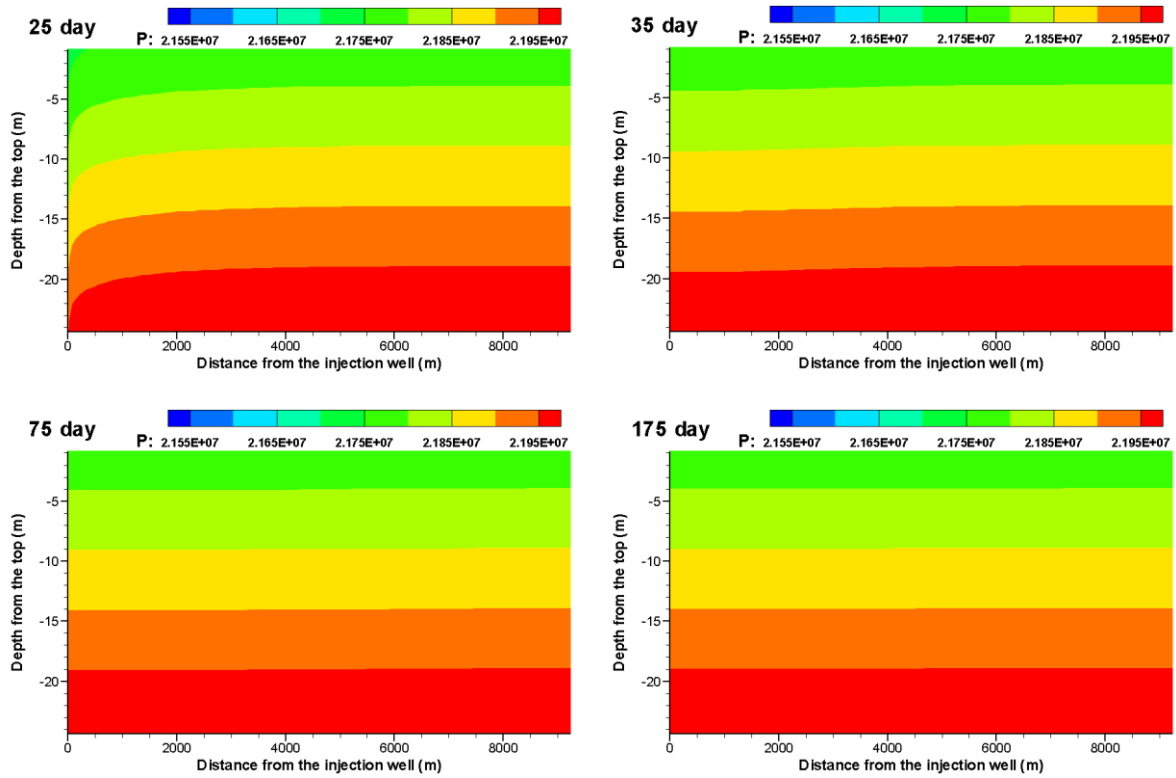
Figure 5.5 The pressure change characteristics after stopping the saline production

Saline push of 1,000 m^3 for 25 days with constant flow (40m^3/d). The pressure change characteristic during the saline push are shown in Figure 5.6.
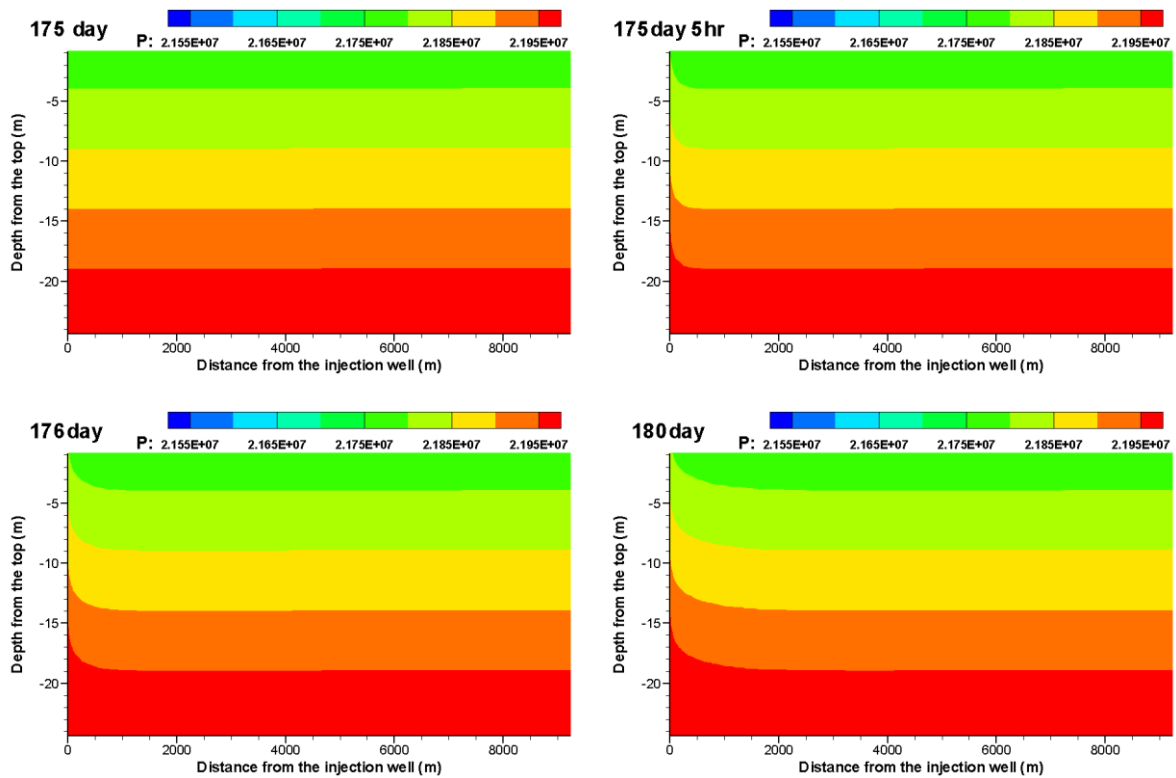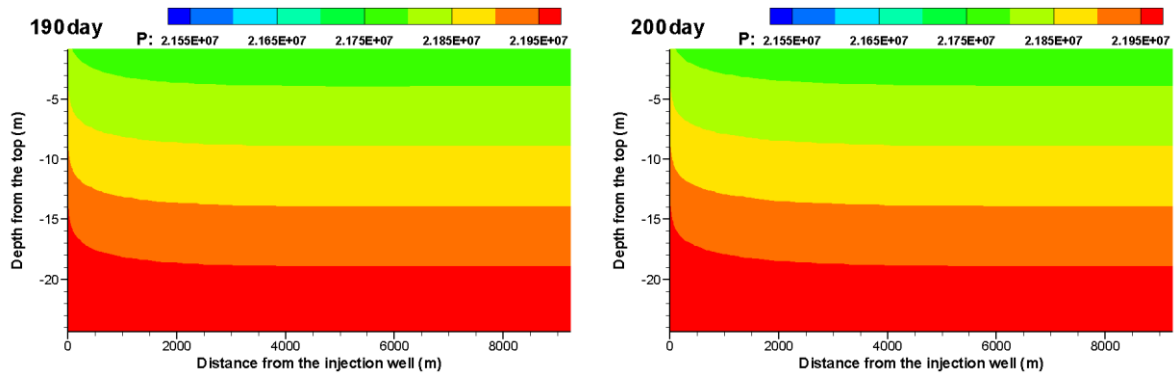
Figure 5.6 The pressure change characteristics during the saline push

100 days after the saline push stopped, the pressure recovered to its original pressure. The pressure change characteristics are shown in Figure 5.7.
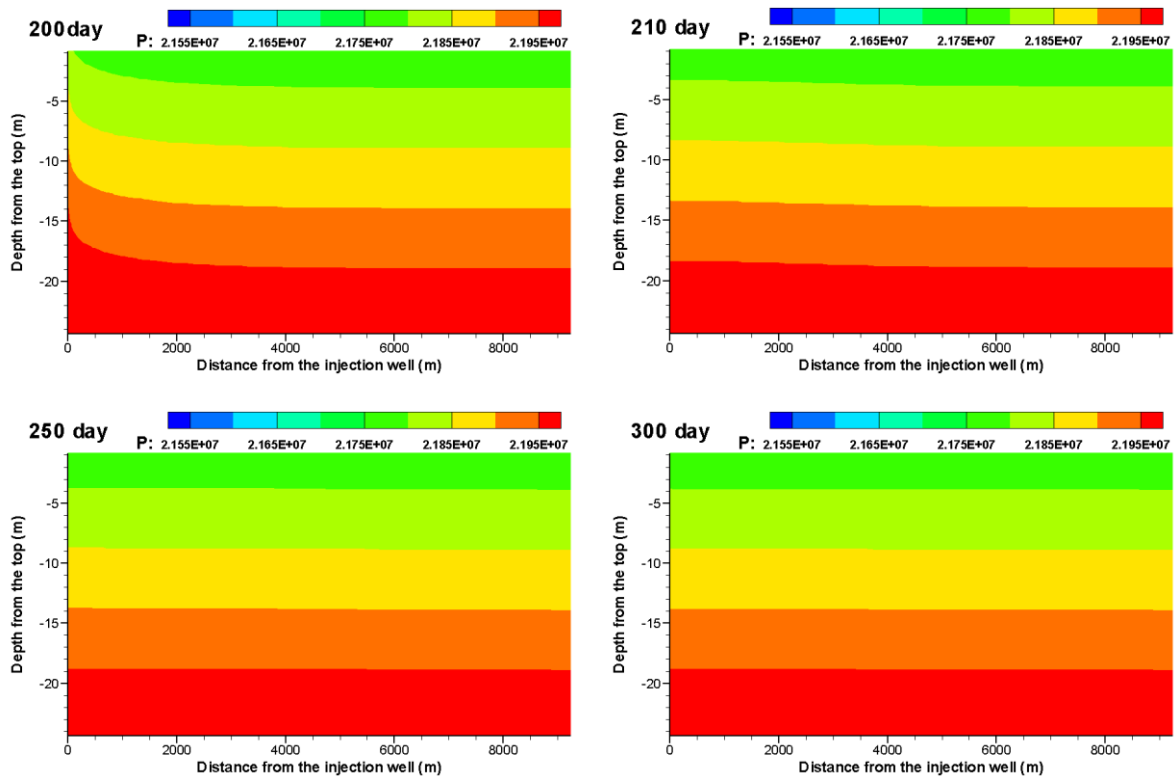
Figure 5.7 The pressure change characteristics after saline push stopped

(2) Second stage

The second stage (case): CO_2 injection of 1,000 t for 25 days with constant flow (40 t/d). The pressure change characteristics in the reservoir during the CO_2 injection are shown in Figure 5.8, and the CO_2 saturation is shown in Figure 5.9.
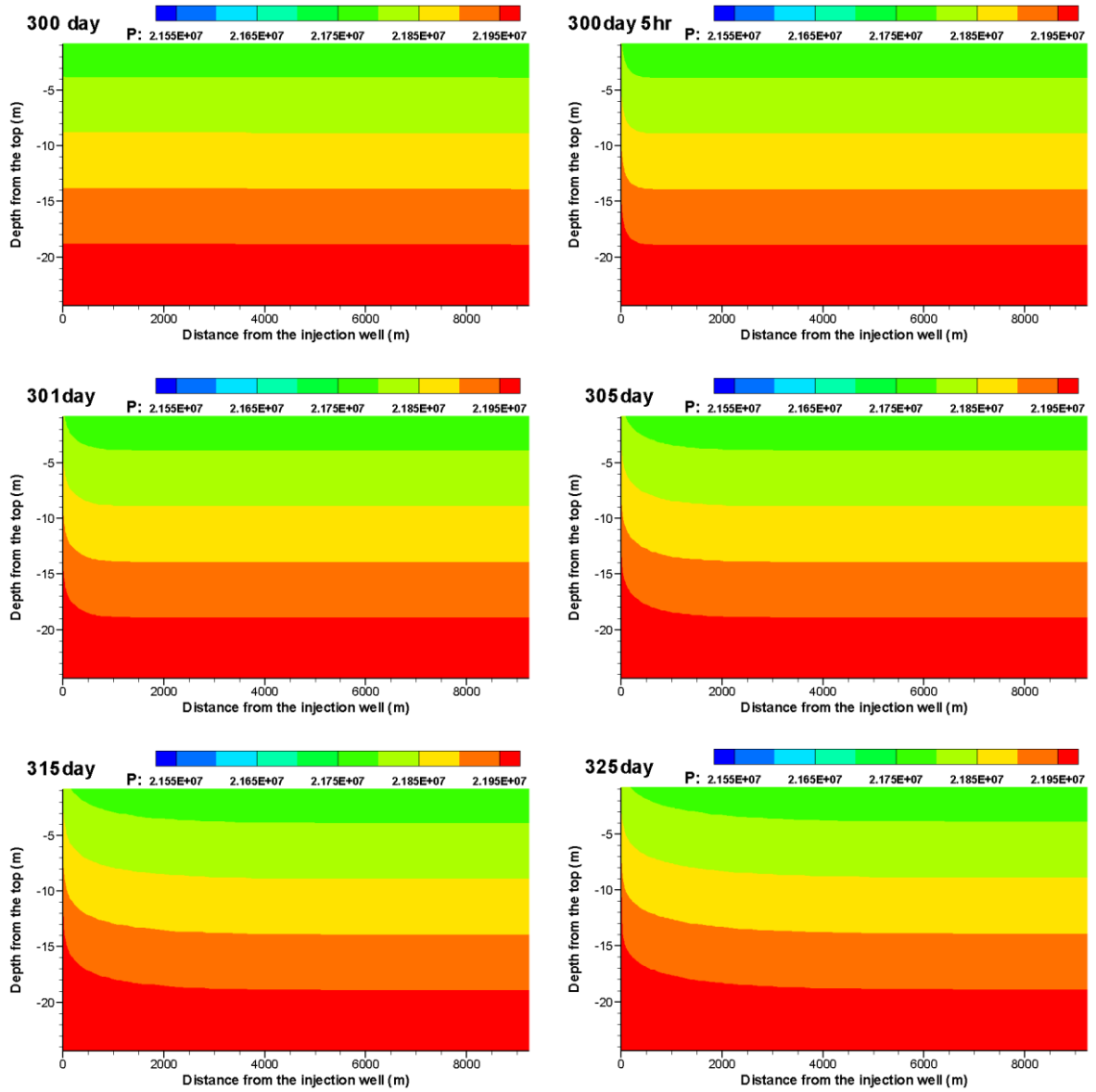
Figure 5.8 The pressure change characteristics during the CO₂ injection
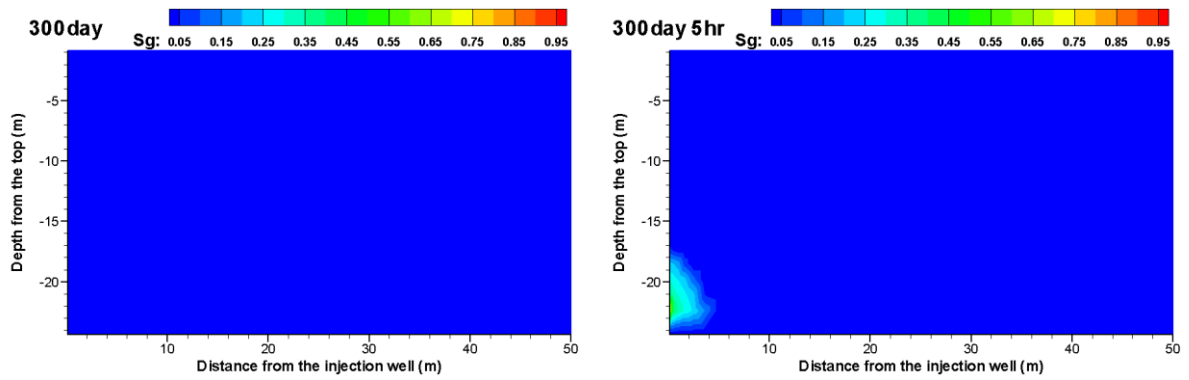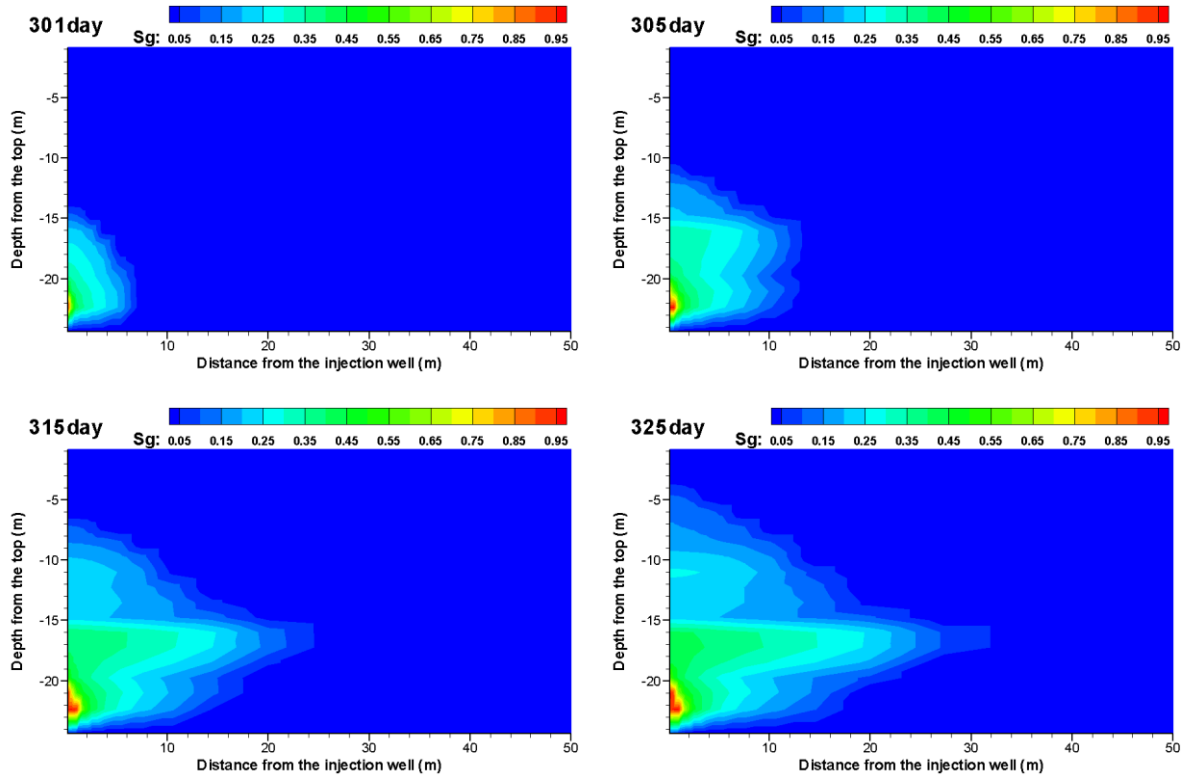
Figure 5.9 The CO$_2$ saturation during the CO$_2$ injection

(3) Third stage

The third stage (case): CO$_2$ and saline mixed liquid pull of 2,000 t for 25 days with constant flow (80m^3/d). The pressure change characteristics during the mixed liquid pull are shown in Figure 5.10, and the CO$_2$ saturation is shown in Figure 5.11.
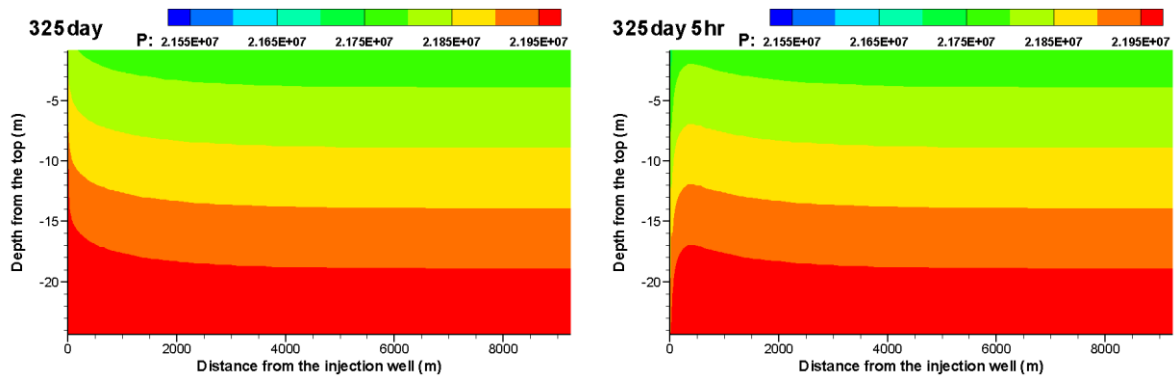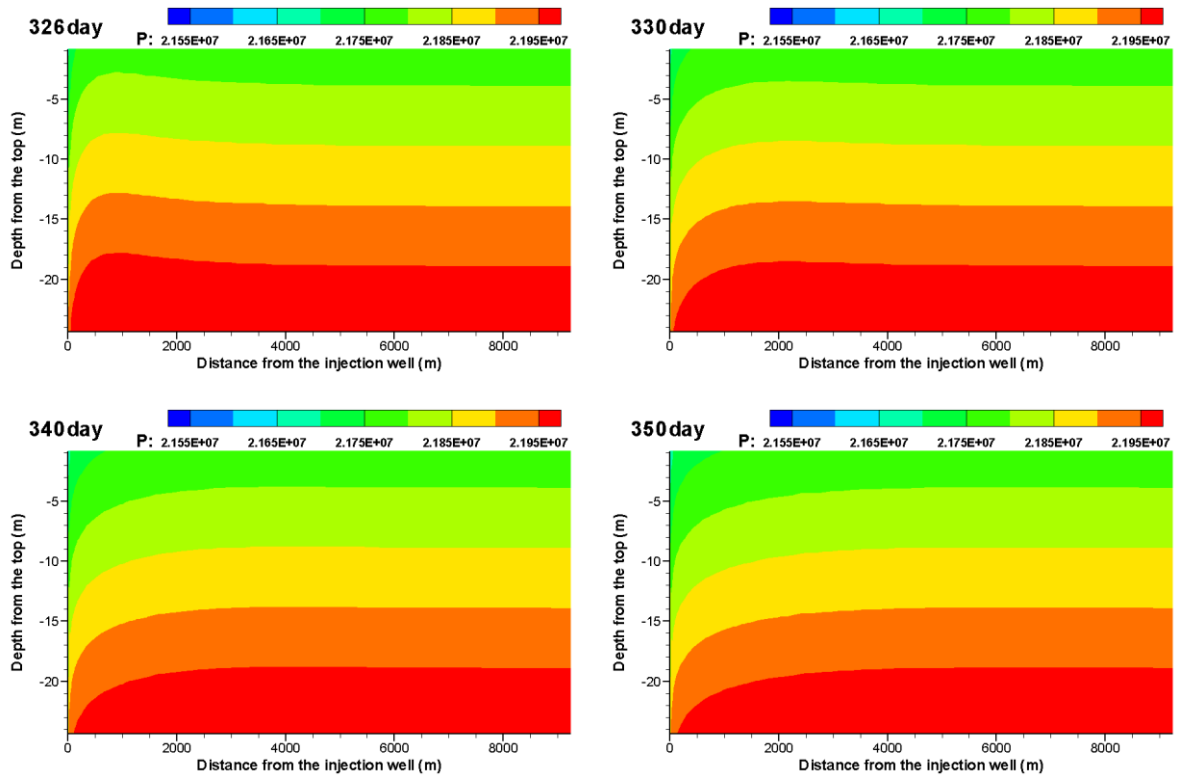
Figure 5.10 The pressure change characteristics during the mixed liquid pull
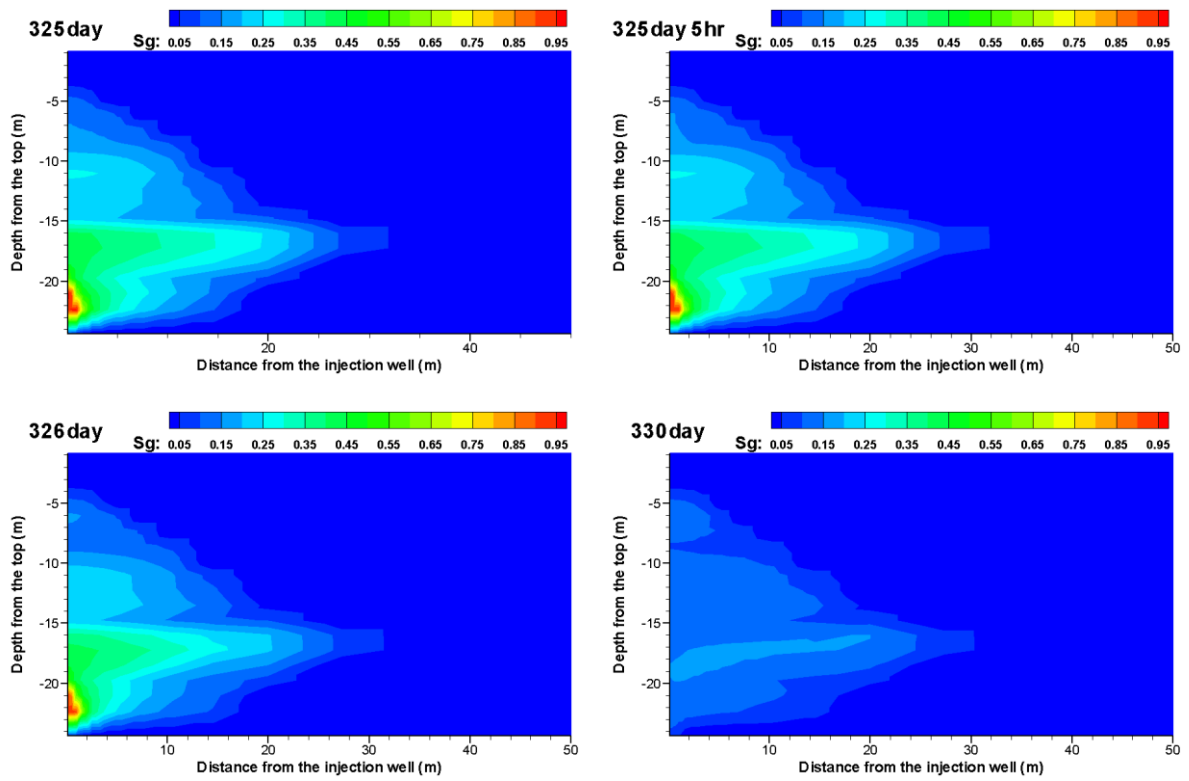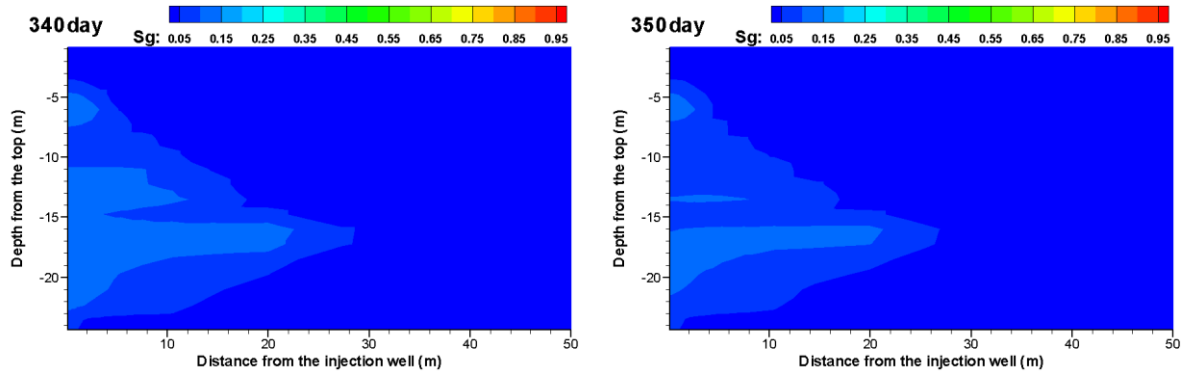
Figure 5.11 The CO$_2$ saturation during the mixed liquid pull

However, the study purposes of the single well test are very limited, and the test results are very difficult to explain. The simulation of the next stage single well test is still ongoing, to optimise the process and clarify the study purposes.

In addition, our Team and Eastern Junggar Oilfield (under Xinjiang Oilfield) are planning to start a multi-well test of CO$_2$-EWR in the Eastern Junggar Basin, including one injection well and four oil production wells (the saline content of produced liquid reaches more than 90%, which may be good for CO$_2$-EWR research). The purpose of this pilot project is to construct a project framework of long-term CO$_2$ geological storage research, similar to the CO$_2$CRC Otway Project.
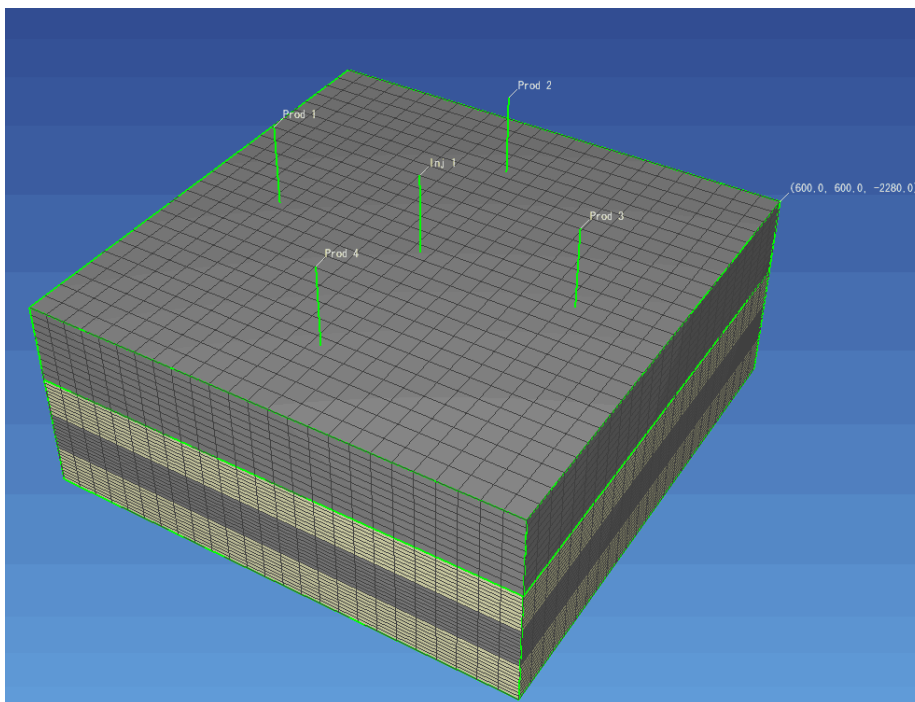
Figure 5.12 Injection well and oil production wells of Cai 9 block
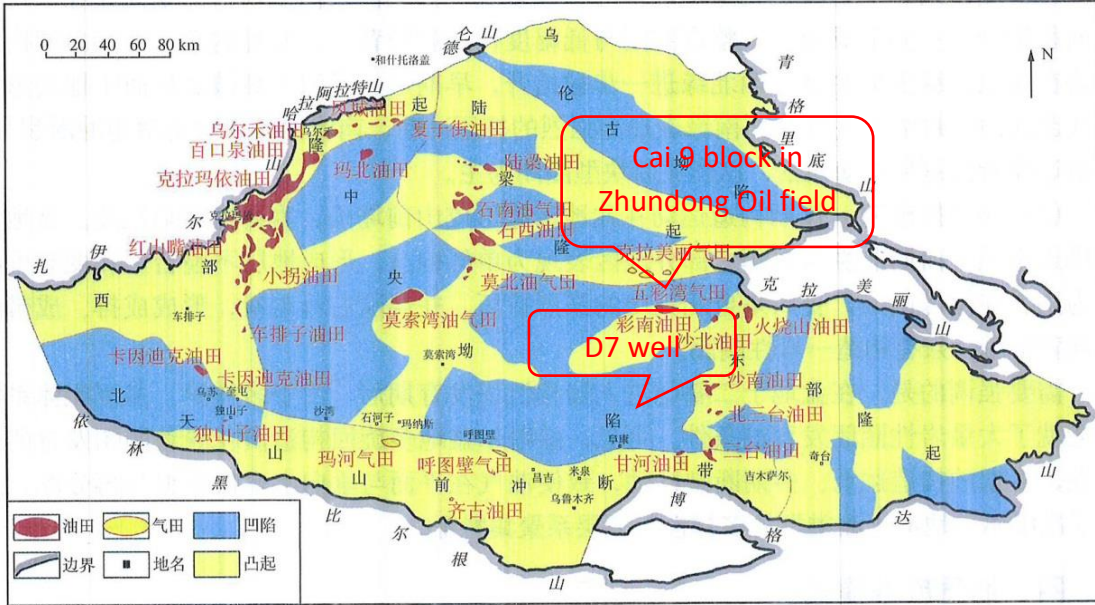
Figure 5.13 Potential storage site (Cai 9 block) in Eastern Junggar Oilfield

6. ECONOMIC FEASIBILITY ANALYSIS AND RISK ASSESSMENT

6.1 PRELIMINARY ECONOMIC ANALYSIS

The recommended demonstration site has good geological conditions and the reservoir has good permeability and porosity. The desalinated deep salt water is transported to nearby water demand areas or factories depending on the water quality. The salt water desalination treatment adopts RO technology.

The design target of CO_2-EWR is to inject CO_2 at 1 Mt/a for 30 years. The constraints are the following:

(1) To prevent the risk of leakage of the caprock, the maximum pressure of the saline aquifer must be less than 1.5 times the original formation pressure;

(2) The fluid passing through the wellbore to the bottom must reach supercritical state;

(3) The temperature and pressure in the reservoir during the whole process of CO_2 flooding must always ensure that the CO_2 is in a supercritical state and that phase transition is prevented.

(4) For the 30 year project period, CO_2 must not move to the salt water production well.

Table 6.1 The schematic design of the CO_2-EWR demonstration project

CO_2 compression	CO_2 pipeline transportation	CO_2-EWR	Extracted water desalination
0.10 MPa to pipe inlet pressure (12 MPa), 5-stage compression and one-stage pump	Dense CO_2 pipeline, 12 Mpa of inlet pressure	Injection wells with water production well (or pressure control well), storage parameters shown in Table 6.2	RO technology

Table 6.2 Basic technical parameters of CO_2-EWR storage

Storage scale	1 Mt /yr
Project period	30 years
Reservoir depth	2100 m
Sand thickness	300 m
Horizontal permeability (Kh)	150 mD
The number of injection wells and production wells	1 injection well, 1 production well
The number of new wells	2
Injection rate	3424.66 t/d

CO_2 saline aquifer storage costs are primarily divided into capital cost and operation and management (O&M) costs. The capital cost of storage mainly includes the costs of field investigation and site evaluation, well drilling, injection equipment and monitoring equipment.

Field investigation and site evaluation: the basic geological conditions of the primary storage site and a certain range within the surrounding area need be evaluated. The key points of evaluation are formation characteristics, faults and attitude of stratum. The methods include 2D and 3D seismic survey and drilling, etc, of which the cost is mainly construction cost and data interpretation fees.

Well drilling: includes injection wells, production wells, and monitoring and pressure control wells. It is very important to calculate the number of wells to be drilled because of the high cost. The construction cost consists of well drilling, well completion, logging, and well cementation cost, as well as some monitoring costs.

Injection equipment cost: mainly includes the costs of workshop building, electrical service, power distribution lines, injection pipeline and well site connection, etc.

O&M cost mainly includes: normal daily expenses (O&Mdaily), consumables (O&Mcons), surface equipment maintenance (O&Msur), subsurface maintenance (O&Msubsur), monitoring cost, and CO_2 pressure boost, etc.

The cost of brine treatment includes desalination costs and the income from selling desalinated brine to industry. This paper takes no account of the desalinated brine transportation cost. Due to the limited geological data, the saltwater production temperature and TDS is still uncertain. The desalination cost is temporarily calculated at 1.5 USD/t CO_2 (IAEA, 2013).

The basic cost evaluation parameters of this Project are shown in Table 6.3, and the cost outcomes are shown in Table 6.4.

Table 6.3 Basic cost evaluation parameters

Storage scale（Mt /yr）	1
Project period（year）	30
Discount rate (%)	0.1
Electricity price (USD /kW.h)	0.083
Industrial water price（USD /t water）	0.54
Desalination price（USD /t CO_2）	1.5

Table 6.4 Storage cost outcomes

Cost structure	Unit	Value
1 Saline aquifer storage		
1.1 Capital cost	**10^4 USD**	**2779.33**
1.1.1 Site screening and evaluation	10^4 USD	1153.85
1.1.2 Equipment cost	10^4 USD	19.02
1.1.3 Drilling cost	10^4 USD	1537.23
1.1.4 Monitoring equipment cost	10^4 USD	69.23
1.2 Operation & Management cost	**10^4 USD/yr**	**96.22**
1.2.1 O&Mdaily	10^4 USD/yr	10.00
1.2.2 O&Mcons	10^4 USD/yr	1.54

1.2.3 O&M$_{sur}$	10^4 USD/yr	7.61
1.2.4 O&M$_{subsur}$	10^4 USD/yr	1.85
1.2.5 $CO_2$$_{compressure}$	10^4 USD/yr	64.46
1.2.6 Monitoring cost	10^4 USD/yr	10.77
1.3 Total storage cost	**10^4 USD**	**5666.06**
1.4 Annual levelised capital cost	10^4 USD/yr	294.83
1.5 Annual total cost	10^4 USD/yr	391.05
1.6 Storage levelised cost	USD/t CO_2	3.91
2 Desalination treatment	**10^4 USD**	**68.15**
2.1 Desalination cost	10^4 USD	150.00
2.2 Income from desalinated brine sale	10^4 USD	81.85
2.3 Desalination levelised cost	USD/t CO_2	1.50
3 Comprehensive levelised cost of storage and desalination	**USD/t CO_2**	**5.41**
4 CO_2 compression levelised cost	USD/t CO_2	12.50
5 CO_2 pipeline transportation levelised cost	USD/t CO_2	1.97
6 Total levelised cost	**USD/t CO_2**	**19.88**

Note: The cost calculation does not include other fixed assets and pre-project investments, such as compensation, road and infrastructure, environmental assessment, safety evaluation, etc.

6.2 THE STORAGE RISK ASSESSMENT

An overall risk and cross-risk assessment of the Project has been performed, based on the environmental risk assessment guidelines of the Ministry of Environmental Protection and the classification criteria of Hnottavange -Telleen (GHG Underground).

Figure 6.5 Overall risk and cross-risk assessment of the demonstration project

Reference number	Risk	Whole project (W), Capture (C), Transportation (T) or Storage (S)	Political, Economic or Technical	Start-up				Operation			Closure	Post-Closure	CO$_2$-EWR risk			Notes
				Opportunity	Planning	Engineering	Construction	Capture	Transportation	Injection			Consequences （1~5）	Likelihood （1~5）	Controlability （1-5）	
1	Legal uncertainties (including pore space ownership)	W	Political	X	X	X	X	X	X	X	X	X	1	1	4	No oilfields on the storage site; no ownership problem.
2	Uncertain cost or regulations for integrated project, e.g. plugging	W	Political								X		2	4	2	Domestic CCUS related laws and regulations are not complete.

	and abandonm ent (closure/p ost closure)														
3	Public engageme nt (public opposition , risk communic ation, public disclosure of data, etc.)	W	Political	X	X	X	X	X	X	X		1	2	3	Low population density.
4	Project permits not obtained	W	Political	X	X	X	X	X	X	X	X	1	1	1	No precedent for demonstration projects to be licensed in China.
5	Lack of financial driver e.g.,	W	Economi c			X	X	X	X	X		3	4	3	Large CO_2 price fluctuation

#	Factor		Category														Comment
	CO₂ price/credit, benefit (oil or other products)																affects project operation.
6	Insufficient project financial resources- cost of capital	W	Economic	X	X								4	3	3	Increasing financing channels and seeking financial support can effectively reduce risks.
7	Unexpected construction or operational cost changes	S	Economic			X	X	X	X	X	X		2	3	2	
8	Uncertainty in CO₂ supply	W	Economic					X	X	X			2	3	3	The other emission sources are relatively far away.

No	Risk	Type	Category										P	I	R	Comment
9	Lack of emissions accounting	W	Economic, Political			X	X	X	X	X			1	3	1	Very low impact on this project.
10	Technology scale-up	W	Technical			X	X	X	X	X			2	3	1	Lack of experiences of similar projects.
11	Lack of knowledge /qualified resources for operating the unit	W	Technical	X	X	X	X	X	X	X		X	3	4	5	The right team and enhancing training could reduce this risk.
12	Project impacts on environment	W	Technical				X	X	X	X	X	X	3	2	4	It is mainly the pollution of groundwater, and it has good controllability under the premise of complete environmental assessment.
13	External natural	W	Technical					X	X	X	X	X	1	2	3	Limited impact.

No.	Risk	Type	Category															Description
	impacts on project																	
14	External man-made impacts on project	W	Technical					X	X	X	X	X			2	3	4	It mainly affects the pipeline and surface facilities. Enhancing communication, increasing warning signs, and regularly checking could reduce the risk.
15	Site planning uncertain, conflict with other usage rights	W	Technical				X	X	X	X				3	1	5	The business entity and the holder of the site usage rights are the same.
16	Accidental or intentional interruption or	C⇆T⇄S	Technical					X	X	X				1	3	3	The chemical plant as a CO_2 emission source is stable.

	intermittency of CO_2 supply, CO_2 in-take or transportation																		
17	Shared infrastructure by multiple projects (uncertain ownership, performance or lack of coordination)	C⇆T⇄S	Technical					X	X	X			2	1	5	No public facilities.
18	Using existing facilities (especially pipeline: knowledge of conditions,	C⇆T⇄S	Technical		X	X	X		X	X			2	3	5	Most facilities should be newly built.

	obligation to other users, CO_2 or material specifications, uncertain timing)															
19	Unintended phase change	C⇆T⇄S	Technical					X			1	5	4	The surface is relatively flat, and the possible phase transition occurs in the pressure relief process, with minimal consequences.
20	CO_2 out of specifications: source gas composition is not as expected CO_2	C→T→S	Technical					X			3	3	3	Good controllability.

21	Mismatched component performance (capacity, resource, flexibility, efficiency, well integrity, usage life)	C⇆T⇄S	Technical							X	X	X			3	3	4	Good controllability.
22	Lower capture efficiency due to the upstream plant flexible operation	C→T→S	Technical							X					2	2	3	Large potential storage capacity in this site.
23	Insufficient storage resource	S→T→C	Technical							X	X	X			3	3	4	

67

#	Description		Type														Comment
24	Reservoir does not perform as predicted (injectivity reduction, storage resource, geomechanical stability, containment)	S→T→C	Technical	X	X	X	X			X		X	3	3	3	More reservoir data can be obtained in the next stage, which could improve model precision.
25	Model uncertainties regarding the storage performance (capacity/injectivity/containment)	S→T→C	Technical					X	X	X			4	3	5	Knowledge sharing can improve the deficiency of this aspect, and the controllability is very high.
26	Lack of maintenan	C⇆T⇄S	Technical					X	X	X			2	2	4	Taking appropriate

	ce and emergency control procedures/ Safety related accident															measures can minimise this risk.

7. CONCLUSIONS

(1) The CO_2 emission sources in the Junggar Basin are mainly concentrated in the Urumqi, Shihezi and Kuitun regions. The carbon emissions of a total number of 54 sources in the Basin amount to 132.22 Mt. Power plants account for over 50% both in quantity and annual emissions share – there are as many as 32 plants with total emissions of 67.51 Mt/a. There are 5 cement plants in this region, with emissions of 28.05 Mt/a, and 12 chemical plants, including coal chemical and petrochemical plants, with emissions of about 22.13 Mt/a.

(2) In China, the Junggar Basin has the greatest potential for CCS development, as it has significant carbon emissions together with deep saline aquifers having good geology for CO_2 geological storage or CO_2-EWR. By using the formula proposed by USDOE and other authoritative papers, we evaluated the potential of CO_2 geological utilisation and storage in the Junggar Basin. The results show that the potential of CO_2 storage by using CO_2-EWR or deep saline aquifer CO_2 storage technologies is greatest (about 480.27×10^8-1640.93×10^8t (960.55×10^8t average expected)) because of the large area of the Basin, thick saline aquifers and suitable geological security conditions. The potential of CO_2 storage by using other technologies is much lower, for example, the potential by using CO_2-EOR is just 1.48×10^8t, while the potential of depleted oil field CO_2 storage is 13.45×10^8t. However, both of these figures are more credible than CO_2-EWR or deep saline aquifers CO_2 storage, because of the extent of geological surveying and data support.

(3) The source-sink matching results are very good for CO_2-EWR or standalone CO_2 geological storage in the Junggar Basin. All CO_2 sources could be matched to suitable storage targets within 50 kilometers. Furthermore, Western Junggar Basin is suitable for CO_2-EOR demonstration projects, while Eastern Junggar Basin is suitable for CO_2-EWR demonstration projects.

(4) Funded by the CAGS and China Geological Survey (CGS) project "Geological Survey of CO_2 Geological Storage in the Junggar and Other Typical Basins", we completed outcrops geological surveys, 2D seismic exploration and downhole reservoir testing for reservoir characterisation of CO_2-EWR, and ultimately three perforated layers were selected for next stage study. Based on the geological data, we built a 3D static geological model of the storage site by using PETREL software, and we inferred that the total volume of rock is 3.2551×10^{10} m^3, while the total volume of pores is 4.327×10^9 m^3, which could be regarded as the total theoretical groundwater resources volume. Furthermore, we evaluated the capacity of CO_2 storage by using the formula proposed by USDOE (2007), which is 71.97 Mt at a P50 level.

(5) In order to study the enhanced efficiency of CO_2 storage and saline production in the D7 well, we built a homogenous horizontal 3D geological model for numerical simulation covering 20 km × 20 km. From the geology of reservoirs and the numerical simulation results, we concluded that CO_2-EWR technology could greatly improve the efficiency and total amount of CO_2 storage and saline production. In the D7 well storage site, the sandstone layer at the depth of 2,246.5 - 2,265 m is the best reservoir for the next stage push-pull test.

(6) The recommended emission source for CO_2-EWR demonstration is Guanghui New Energy Co., Ltd and the storage site is located at Suosuoquan Depression in the Eastern Junggar Basin. According to the preliminary economic analysis, the fixed capital cost is $2,779.33*10^4$ USD, Operation and Management cost is $96.22*10^4$ USD/yr, and the comprehensive levelised cost of storage and desalination is 5.41 USD/t CO_2.

REFERENCES

Aines R D., Wolery T. J. , Bourcier W L, Wolfe T, Hausmann Chris. Fresh water generation from aquifer-pressured carbon storage: Feasibility of treating saline formation waters, Energy Procedia 4, 2011: 2269-2276.

Angela Goodman, U.S. DOE methodology for the development of geologic storage potential for carbon dioxide at the national and regional scale, International Journal of Greenhouse Gas Control, 2011: 952-965.

Angela Goodman and Alexandra Hakala, U.S. DOE methodology for the development of geologic storage potential for carbon dioxide at the national and regional scale. International Journal of Greenhouse Gas Control, 2010: 952-65.

Bert M, IPCC special report on CO_2 capture and storage, London: Cambridge University Press, 2005.

Buscheck T A, Sun Y, Hao Y, Wolery T J, Bourcier W, Tompson A F, et al., Combining brine extraction, desalination, and residual-brine reinjection with CO_2 storage in saline formations: implications for pressure management, capacity, and risk mitigation, Energy Procedia 4, 2011: 4283–4291.

Court B, Celia M A, Nordbotten J M, Elliot T R, Active and integrated management of water resources throughout CO_2 capture and sequestration operations, Energy Procedia 4, 2011: 4221–4229.

Carbon Sequestration Leadership Forum (CSLF), Estimation of CO_2 storage capacity in geological media, June 2007: 43.

Davidson C L, Dooley J. J., Dahowski R. T, Assessing the impacts of future demand for saline groundwater on commercial deployment of CCS in the United States, Energy Procedia 1, 2009: 1994-1956.

Greenhouse Gas R&D Program, Development of storage coefficients for carbon dioxide storage in deep saline formations. IEA. 2009.

Holloway S, Underground sequestration of carbon dioxide available greenhouse gas mitigation option, Energy Conversion and Management, 2005: 231-333.

Holtz M H, Residual gas saturation to aquifer influx: a calculation method for 3-D computer reservoir model construction, Society of Petroleum Engineers, Kuala Lumpur Malaysia. SPE Paper, 75502, 2002.

Hunter K, Bielicki J M, Middleton R, Stauffer P, Pawar R, Harp D, Martinez D, Integrated CO_2 Storage and Brine Extraction, Energy Procedia 114, 2017: 6331 – 6336.

IEA Greenhouse Gases R&D Programme (IEA GHG),Opportunities for Early Application of CO_2 Sequestration Technology. IEA GHG Report PH4/10, 2002.

Kobos P H., Cappelle M A., Krumhansl J L., Dewers T A, McNemar A, Borns D J, Combining power plant water needs and carbon dioxide storage using saline formations: Implications for carbon dioxide and water management policies. International Journal of Greenhouse Gas Control 5, 2011: 899–910.

Li Q, Wei Y, Liu G, Lin Q, Combination of CO_2 geological storage with deep saline water recovery in western China: Insights from numerical analyses, Applied Energy 116, 2014: 101–110.

Li Q, Wei Y, Liu G., Shi H, CO_2-EWR: a cleaner solution for coal chemical industry in China. Journal of Cleaner, Production 103, 2015: 330-337.

Li Y, Fang Q, Ke Y, Dong J, Yang G, Ma X, Effect of high salinity on CO_2 geological storage: a case study of qianjiang depression in jianghan basin, Earth Science-Journal of Chinese University of Geoscience, 2012, 37(2): 283-288.

N. Wei, and et al, J. CO_2 Util.http://dx.doi.org/10.1016/j.jcou.2014.12.005.

Oldenburg C M, Screening and ranking framework for geologic CO_2 storage site selection on the basis of health, safety and environmental risk, Environmental Geology, 2008, 54(8): 1687-1694.

Dahowski R T, Dooley J J, Davidson C L, Bachu S and Gupta N, 2005. Building the Cost Curves for CO_2 Storage: North America. Technical Report, IEA Greenhouse Gas R&D Programme, 2005/3.

Stefan Bachu, Review of CO_2 storage efficiency in deep saline aquifers, International Journal of Greenhouse Gas Control, 2015: 188-202.

Surdam R C, Jiao Z, Stauffer P, Miller T, The key to commercial-scale geological CO_2 sequestration: Displaced fluid management. Energy Procedia 4, 2011: 4246-4251.

USDOE (U.S. Department of Energy, Office of Fossil Energy), Carbon Sequestration Atlas of United States and Canada, 2007: 86.

Li X, and Y Liu, CO_2 Point Emission and Geological Storage Capacity in China, 2009: 2793-2800.